

# A three-dimensional description of shape memory alloy thermomechanical behavior including plasticity

Sergio A. Oliveira<sup>1</sup> · Marcelo A. Savi<sup>2</sup> · Nestor Zouain<sup>2</sup>

Received: 17 September 2015 / Accepted: 9 December 2015 / Published online: 21 January 2016  
© The Brazilian Society of Mechanical Sciences and Engineering 2016

**Abstract** This paper introduces a novel three-dimensional constitutive model that describes the thermomechanical behavior of shape memory alloys (SMAs). The model is developed within the framework of continuum mechanics and the standard generalized materials. Four macroscopic phases are considered associated with austenite and three variants of martensite. Phase transformations can be induced by temperature, volumetric and deviatoric strains. The description of plasticity is also of concern assuming kinematic and isotropic hardening. Numerical simulations are carried out showing that the proposed model is able to capture the general thermomechanical behavior of SMAs for uniaxial and multiaxial tests, even in situations with complex thermomechanical loading paths.

**Keywords** Shape memory alloys · Smart materials · Constitutive model · Plasticity · Numerical simulation · Phase transformations

---

Technical Editor: Francisco Ricardo Cunha.

---

✉ Marcelo A. Savi  
savi@mecanica.coppe.ufrj.br

Sergio A. Oliveira  
amserol@yahoo.com.br

Nestor Zouain  
nestor@ufrj.br

<sup>1</sup> Department of Mechanical Engineering, CEFET/RJ, Rio de Janeiro, RJ 20.271.110, Brazil

<sup>2</sup> Center for Nonlinear Mechanics, COPPE - Department of Mechanical Engineering, Universidade Federal do Rio de Janeiro, P.O. Box 68.503, Rio de Janeiro, RJ 21.941.972, Brazil

## List of symbols

$B^+$	Thermodynamic force related to the volume fraction due to positive detwinned martensite
$B^-$	Thermodynamic force related to the volume fraction due to negative detwinned martensite
$B^A$	Thermodynamic force related to the volume fraction due to austenite
$E_{ijkl}$	Elastic tensor
$E_{ijkl}^A, E_{ijkl}^M$	Elastic tensor for austenitic and martensitic phases
$G$	Shear modulus
$H$	Kinematic hardening modulus
$H^A, H^M$	Kinematic hardening modulus of austenite and martensite
$I_{\Theta}$	Indicator function associated with the convex set $\Theta$
$I_{\pi}$	Indicator function associated with the convex $\pi$
$I_{\chi}$	Indicator function of the convex set $\chi$
$I_f$	Indicator function associated with yield surface (classical plasticity)
$K$	Isotropic plastic modulus
$L_0^+, L^+$	Parameters related to the critical stress due to positive detwinned martensite phase
$L_0^-, L^-$	Parameters related to the critical stress due to negative detwinned martensite phase
$L_0^A, L^A$	Parameters related to the critical stress due to the austenitic phase
$q_j$	Heat flux
$r_{ij}$	Second-order tensor defined from the loading history

$T$	Temperature				
$T^A$	Temperature above with the austenitic phase is stable				
$T^M$	Temperature below with the martensitic phase is stable	$\eta^I$			martensite, negative detwinned martensite and austenite)
$T_0$	Reference temperature in a stress-free state	$\eta_{ij}^k$			Parameter that defines the coupling between the phase transformation and isotropic hardening
$T^F$	Reference temperature to determine the yield strength at high temperatures				Parameter that defines the coupling between the phase transformation and kinematic hardening
$X_{ij}$	Thermodynamic force associated with the plastic strain tensor	$\lambda, \mu$ $\lambda^A, \lambda^M$			Lamé coefficients Lamé coefficients referring to austenite and martensite
$Y$	Thermodynamic force associated with the isotropic hardening	$\mu^A, \mu^M$			Lamé coefficients related to austenite and martensite
$Z_{ij}$	Thermodynamic force associated with the kinematic hardening tensor	$\Phi$ $\Phi^M$			Pseudo-potential of dissipation Mechanical part of the pseudo-potential of dissipation
$\alpha$	Parameter that controls the stress–strain hysteresis loop height	$\Phi^H$			Mechanical part of the pseudo-potential of dissipation
$\alpha_{ijkl}^h$	Fourth-order tensor that controls the stress–strain hysteresis loop width	$\psi$			Helmholtz free energy density
$\alpha_N^h, \alpha_s^h$	Normal and shear components of the tensor $\alpha_{ijkl}^h$	$\psi^+, \psi^-, \psi^A, \psi^M$			Helmholtz free energy density of isolated phases (positive detwinned martensite, negative detwinned martensite, austenite and twinned martensite)
$\Lambda^A, \Lambda^M$	Phase transformation temperature functions related to austenite and martensite				
$\Lambda, \Lambda^N$	Phase transformation temperature functions	$\Gamma$			Equivalent strain field
$\beta^+$	Volume fraction related to the positive detwinned martensite	$\nu$ $\nu^A, \nu^M$			Poisson's ratio Poisson's ratio associated with austenite and martensite
$\beta^-$	Volume fraction related to the negative detwinned martensite	$\Omega_{ij}$			Tensor related to the thermal expansion coefficients
$\beta^A$	Volume fraction referring to austenite	$\Omega_{ij}^A, \Omega_{ij}^M$			Tensor related to the thermal expansion coefficients of the austenite and martensite
$\beta^M$	Volume fraction related to the twinned martensite				
$\beta_s^+, \beta_s^-$	Volume fraction associated with the starting of phase transformation process	$\tau$			Set related to subdifferential associated with the convex set $\pi$ (tetrahedron)
$\varepsilon_{ij}$	Total strain tensor	$\Upsilon$			Set related to subdifferential associated with the convex set $\chi$
$\hat{\varepsilon}_{ij}$	Deviatoric strain tensor				
$\varepsilon_{ij}^e$	Elastic strain tensor				
$\varepsilon_{ij}^p$	Plastic strain tensor				
$\varepsilon_{ij}^t$	Phase transformation strain tensor				
$\vartheta$	Internal variable associated with isotropic hardening				
$\zeta_{ij}$	Internal variable associated with kinematic hardening				
$\rho$	Density				
$\sigma_{ij}$	Stress tensor				
$\hat{\sigma}_{ij}$	Deviatoric stress tensor				
$\sigma^Y$	Yield stress				
$\sigma_Y^A, \sigma_Y^M$	Yield stress of the austenitic and martensitic phases				
$\sigma_{A,i}^Y, \sigma_{A,f}^Y$	Yield stress at temperature $T^A$ and $T^F$				
$\gamma$	Plastic multiplier				
$\eta^+, \eta^-, \eta^A$	Parameter associated with the internal dissipation (positive detwinned				

## 1 Introduction

Smart material systems and structures have considerable importance nowadays being related to the design of adaptive systems that can mimic some aspects of natural systems. In general, it is possible to understand smart material properties as the coupling between different physical fields as mechanical, electrical, magnetic, among others. In this regard, several materials have been investigated and it is important to highlight shape memory alloys (SMAs), piezoelectric materials, magneto-strictive materials and electro-magneto rheological fluids.

SMAs have remarkable properties related to solid phase transformations, being usually employed in applications where large forces and/or displacements are required with

low power consumption. In general, SMAs are being used in biomedical devices, aerospace and robotics applications, civil and mechanical engineering. A discussion about SMA applications can be found in the following references: Lagoudas [23], Paiva and Savi [37], Machado and Savi [27] and Kalamkarov and Kolpakov [21]. Dynamical applications are also employing SMAs exploiting either dissipation capacity or property changes due to phase transformations. Savi [50] presented a general overview of SMA dynamical applications, highlighting the complex response related to these systems. In this regard, it is important to mention applications related to rotordynamics [53], impact systems [43, 55], vibration absorbers [48], adaptive structures [7, 15, 45, 46, 49], and the control of such systems [8, 14].

The thermomechanical behavior of SMAs is very complex, presenting typical responses as pseudoelasticity, shape memory effect and phase transformation due to temperature variations, but also other interesting behaviors as the internal subloops due to the incomplete phase transformations, two-way shape memory effect, plasticity, transformation-induced plasticity and rate dependence [52]. All these phenomena justify the numerous researches related to the modeling, simulation and experimental analysis of SMAs.

The macroscopic constitutive modeling of SMAs relies on the continuum thermodynamics with internal state variables to take into account the changes in the microstructure due to phase transformation [37, 40]. Lagoudas [23] and Paiva and Savi [37] presented a general overview of the SMA modeling with the emphasis on the phenomenological constitutive models.

The three-dimensional description of the SMA thermomechanical behavior is even more complex. Besides the large number of complex phenomena involved, difficulties related to experimental tests introduce more troubles for a proper description. Experimental analyses related to multiaxial tests are essential for the comprehension of SMA behavior. In this regard, it is important to highlight several research efforts related to this general objective: Auricchio et al. [5], Wang et al. [63], Grabe and Bruhns [19], McNaney et al. [29], Manach and Favier [28], Sittner et al. [59, 58]. Recently, an international effort was developed in order to evaluate all details about thermomechanical behavior of SMAs: Roundrobin SMA Modeling. Sittner et al. [56] reported some activities that compare capabilities of different models, establishing a proper relation with experimental data. In general, experimental tests consider coupled tension–torsion tests to characterize the general three-dimensional thermomechanical behavior of SMAs.

The description of three-dimensional behavior of SMAs is the nowadays challenge that is involving several researches. Lagoudas et al. [24] proposed several improvements to the model due to Boyd and Lagoudas [9]. Numerical simulations were carried out showing both tension and tension–torsion tests. Andani and Elahinia [2] investigated the rate-dependent

description of tension–torsion behavior of SMAs employing a modified version of the model due to Lagoudas et al. [24]. Andani et al. [3] described the pseudoelastic behavior of SMA bars and tubes subjected to tension–torsion loadings. Finite difference method is employed to the numerical simulations. Chapman et al. [11] investigated torsional behavior of SMAs considering both one and three-dimensional models. Finite element method was employed for numerical simulations. Panico and Brinson [39] proposed a three-dimensional model that is capable to reproduce the main features related to SMAs both in one and three-dimensional behavior.

Auricchio et al. [5] proposed a three-dimensional model including permanent inelastic effects combined with the description of pseudoelastic and shape-memory behaviors. Brocca et al. [10] proposed a model that has the ability to represent SMA behavior subjected to nonproportional loading paths. Souza et al. [59] developed a model inspired in elasto-plastic theory presenting results for tension–torsion behavior. Tokuda et al. [61, 62] presented a mechanical model of polycrystalline SMA constructed under the assumption of crystal plasticity and deformation mechanisms. Multiaxial loadings are evaluated with the corresponding mesoscopic constitutive equations. Arghavani et al. [4] used a measure of the amount of stress-induced martensite as scalar internal variable and the preferred direction of variants as independent tensor. Popov and Lagoudas [40] presented a model that addressed not only the martensitic transformation between austenite and detwinned martensite but simultaneously considers the detwinning of self-accommodated martensite in polycrystalline SMAs. Zaki and Moumni [64] showed that the introduction of two state variables (martensitic volume fraction and martensitic orientation strain tensor) is an interesting approach to account several effects exhibited by SMAs subjected to thermomechanical loading. Mehrabi and Kadkhodaei [30] and Mehrabi et al. [31] discussed three-dimensional phenomenological constitutive modeling based on microplane theory. Saleeb et al. [42] is another contribution related to 3D multi-mechanism based SMA modeling framework.

Plasticity is an important issue related to SMA thermomechanical behavior. In general, it is possible to think in two different phenomena: classical plasticity and transformation-induced plasticity (TRIP). A clear distinction can be established between both situations. Classical plasticity arises from applied stress or temperature variation, while TRIP is caused by phase proportions variation—even for low constant stress levels, without reaching the yield surface of the weaker phase involved ([18]; Leblond et al. [25]). From now on, the term plasticity is employed to refer to the classical plasticity.

Plastic behavior of SMAs has been the objective of some research efforts. Khalil et al. [22] presented an experimental investigation showing the interdependent behavior of phase transformation and plasticity on

Fe-based SMAs. Zhou [66] proposed a constitutive model for SMAs undergoing plastic strains. Hartl et al. [20] investigated plastic behavior of SMAs treating the interaction between the phase transformations and the yield surface. Paiva et al. [38] and Baêta-Neves et al. [6] presented the one-dimensional description of the plasticity in SMAs, considering the coupling between the plasticity and the phase transformations.

This article deals with the three-dimensional thermomechanical modeling of shape memory alloys including plasticity. The main goal is a numerical investigation to show the model capabilities to represent the most important features of the macroscopic behavior of SMAs in a qualitative point of view. In this regard, numerical simulations are carried out considering single-point situations that represents a homogeneous SMA sample. Uniaxial and multiaxial tests are of concern involving a variety of situations related to the thermomechanical behavior of SMAs.

The constitutive model is developed within the framework of the continuum mechanics and of the generalized standard materials. On this basis, the second law of thermodynamics guides the general formulation. The model is inspired by a one-dimensional model that is able to describe different thermomechanical behaviors of SMAs in a flexible way, presenting numerical simulations that are in agreement with experimental uniaxial tests [1, 6, 33, 35, 38, 44–46]. Originally, this model is inspired by the Fremond's model [17], implementing several modifications in order to match experimental data. The three-dimensional description using this model was previously addressed in Oliveira et al. [34]. Here, a generalization of the three-dimensional model is presented, including classical plasticity and tensor quantities to represent phase transformation strains. These modifications permit a proper description of thermomechanical behavior of SMA in three-dimensional media, allowing a better match with experimental data. An important difference is the possibility to control the width of stress–strain hysteresis loop. A numerical procedure based on the operator split technique is proposed to deal with nonlinearities of the model. Numerical simulations show that the proposed model is able to capture the general thermomechanical behavior of SMAs for uniaxial and multiaxial tests.

## 2 Constitutive model

The modeling of the thermomechanical behavior of SMAs can be done within the framework of the continuum mechanics and the standard generalized materials, assuming that the thermodynamic state of the material is completely defined by a finite number of state variables. Under this assumption, the

thermomechanical behavior can be described by the Helmholtz free energy density,  $\Psi$ , or alternatively, by the Gibbs free energy density. A pseudo-potential of dissipation,  $\Phi$ , is employed to describe irreversible aspects. The main goal of this formalism is to obtain constitutive equations that automatically satisfy the second law of thermodynamics [12, 13, 26]. In this regard, the Clausius–Duhem inequality motivates the definition of thermodynamic forces from the Helmholtz free energy density, related to each state variable. Dissipation aspects are contemplated by the thermodynamic fluxes defined from the pseudo-potential of dissipation, related to each thermodynamic force.

A brief discussion about this procedure is now presented. Assuming that  $\rho$  is the material density,  $s$  is the specific entropy,  $T$  is the temperature,  $\sigma_{ij}$  is the stress tensor,  $\varepsilon_{ij}$  is the total strain tensor,  $q_j$  is the heat flux,  $x_i$  represents the spatial coordinate and the dot means time derivative, the local form of the Clausius–Duhem inequality is given by the following equation where summation convention is evoked:

$$\sigma_{ij}D_{ij} - \rho(\dot{\Psi} + s\dot{T}) - q_i g_i \geq 0 \quad (1)$$

where it is assumed that  $D_{ij} = \dot{\varepsilon}_{ij} = \frac{1}{2} \left( \frac{\partial v_i}{\partial x_j} + \frac{\partial v_j}{\partial x_i} \right)$  and  $g_i = \frac{1}{T} \frac{\partial T}{\partial x_i}$ .

As a first hypothesis concerning the constitutive modeling, it is assumed that the Helmholtz free energy density is a function of a finite set of variables:

$$\Psi = \Psi(\varepsilon_{ij}, T, \beta) \quad (2)$$

where  $\beta$  represents a set of internal variables. Since  $\dot{\Psi} = \frac{\partial \Psi}{\partial \varepsilon_{ij}} \dot{\varepsilon}_{ij} + \frac{\partial \Psi}{\partial T} \dot{T} + \frac{\partial \Psi}{\partial \beta} \dot{\beta}$ , the Clausius–Duhem inequality is rewritten as follows

$$\left( \sigma_{ij} - \rho \frac{\partial \Psi}{\partial \varepsilon_{ij}} \right) \dot{\varepsilon}_{ij} - \rho \left( s + \frac{\partial \Psi}{\partial T} \right) \dot{T} - \rho \frac{\partial \Psi}{\partial \beta} \dot{\beta} - q_i g_i \geq 0 \quad (3)$$

This form motivates the following definitions of the thermodynamical forces, related to reversible part of the process.

$$\sigma_{ij}^R = \rho \frac{\partial \Psi}{\partial \varepsilon_{ij}}; \quad B = -\rho \frac{\partial \Psi}{\partial \beta}; \quad s^R = -\frac{\partial \Psi}{\partial T} \quad (4)$$

In order to describe irreversible processes, complementary laws are defined from a pseudo-potential of dissipation that is a function of internal variables:

$$\Phi = \Phi(\dot{\varepsilon}_{ij}, \dot{\beta}, \dot{T}, q_i) \quad (5)$$

The thermodynamical formalism establishes that the thermodynamics fluxes, related to irreversible part of the process, are defined as follows [17, 26]:

$$\sigma_{ij}^I = \frac{\partial \Phi}{\partial \dot{\varepsilon}_{ij}}; \quad B = \frac{\partial \Phi}{\partial \dot{\beta}}; \quad s^I = -\frac{\partial \Phi}{\partial \dot{T}}; \quad g_i = -\frac{\partial \Phi}{\partial q_i} \quad (6)$$

Alternatively, thermodynamic fluxes may be obtained from the dual of the potential of dissipation  $\Phi^*(\sigma_{ij}^I, B, s^I, g_i)$  allowing the definitions:

$$\dot{\varepsilon}_{ij} = \frac{\partial \Phi^*}{\partial \sigma_{ij}^I}; \quad \dot{\beta} = \frac{\partial \Phi^*}{\partial B}; \quad \dot{T} = \frac{\partial \Phi^*}{\partial s^I}; \quad q_i = -\frac{\partial \Phi^*}{\partial g_i} \quad (7)$$

On this basis, a complete set of constitutive equations is defined:

$$\sigma_{ij} = \rho \frac{\partial \Psi}{\partial \varepsilon_{ij}} + \frac{\partial \Phi}{\partial \dot{\varepsilon}_{ij}} \quad (8)$$

$$B = -\rho \frac{\partial \Psi}{\partial \beta} = \frac{\partial \Phi}{\partial \dot{\beta}} \quad (9)$$

$$s = -\frac{\partial \Psi}{\partial T} - \frac{\partial \Phi}{\partial \dot{T}} \quad (10)$$

$$g_i = -\frac{\partial \Phi}{\partial \dot{q}_i} \quad (11)$$

If the pseudo-potential  $\Phi$  is a positive convex function that vanishes at the origin, the Clausius–Duhem inequality is automatically satisfied.

The consideration of the thermomechanical couplings must consider the energy conservation equation given by the first law of thermodynamics:

$$\rho \dot{\Psi} = \sigma_{ij} \dot{\varepsilon}_{ij} - \frac{\partial q_i}{\partial x_i} - \rho T \dot{s} - \rho \dot{T} s \quad (12)$$

By considering a single point description, spatial variations are neglected. Besides, a convection boundary condition is assumed. Therefore, the first law of thermodynamics has the following form:

$$\rho c_p \dot{T} = -h(T - T_\infty) + \sigma_{ij}^I \dot{\varepsilon}_{ij} + B \dot{\beta} + T \left[ \frac{\partial \sigma_{ij}^R}{\partial T} \dot{\varepsilon}_{ij} - \frac{\partial B}{\partial T} \dot{\beta} \right] \quad (13)$$

where  $c_p$  is the specific heat at constant pressure,  $h$  is the convection coefficient,  $T_\infty$  is the environmental temperature. The first term on the right side of the equation is the convection term whereas the others are associated with the thermomechanical couplings.

Experimental studies show that there are two possible phases in SMAs: austenite and martensite. In the martensitic phase, different crystallographic orientations define what is known by martensitic variants. Concerning austenitic phase, only one variant exists [51, 65]. The description of three-dimensional thermomechanical behavior of SMAs is usually inspired by one-dimensional models and therefore, a limited number of martensitic variants is employed. The idea is to consider a free energy density

for each macroscopic phase and, afterward, to define a free energy of the mixture. The main goal of the proposed model is to describe a variety of phenomena related to elastoplasticity and solid phase transformations in a flexible way. Therefore, pseudoelasticity, shape memory effect, phase transformation due to temperature variation, internal subloops and plasticity with kinematic and isotropic hardening are of concern considering both uniaxial and multiaxial tests.

### 2.1 Free energy density

The definition of the Helmholtz free energy density considers different expressions for each one of the macroscopic phases. Classical thermo-elasto-plastic equations [16, 26, 54] are adopted together with extra terms that describe the phase transformation phenomenon. Motivated by one-dimensional models, the proposed model considers four macroscopic phases: austenite ( $A$ ); the twinned martensite ( $M$ ), which is stable in the absence of a stress field; and two other phases associated with detwinned martensite,  $M^+$  and  $M^-$ . Basically, it is assumed that the free energy densities are functions of the elastic strain,  $\varepsilon_{ij}^e$ , temperature,  $T$ , isotropic hardening variable,  $\vartheta$ , and kinematic hardening tensor,  $\varsigma_{ij}$ . The definition of these energy densities considers that summation convention is evoked [16].

In the previous equations, subscript  $A$  and  $M$  are related

$$\begin{aligned} M^+ : \rho \Psi^+ (\varepsilon_{ij}^e, T, \vartheta, \varsigma_{ij}) &= \frac{1}{2} (\lambda^M \varepsilon_{kk}^e \varepsilon_{pp}^e + 2\mu^M \varepsilon_{ij}^e \varepsilon_{ij}^e) - \alpha \Gamma - \Lambda^M \\ &\quad - \Omega_{ij}^M (T - T_0) \varepsilon_{ij}^e + \frac{1}{2} K^M \vartheta^2 + \frac{1}{2HM} \varsigma_{ij} \varsigma_{ij} \\ M^- : \rho \Psi^- (\varepsilon_{ij}^e, T, \vartheta, \varsigma_{ij}) &= \frac{1}{2} (\lambda^M \varepsilon_{kk}^e \varepsilon_{pp}^e + 2\mu^M \varepsilon_{ij}^e \varepsilon_{ij}^e) + \alpha \Gamma - \Lambda^M \\ &\quad - \Omega_{ij}^M (T - T_0) \varepsilon_{ij}^e + \frac{1}{2} K^M \vartheta^2 + \frac{1}{2HM} \varsigma_{ij} \varsigma_{ij} \\ A : \rho \Psi^A (\varepsilon_{ij}^e, T, \vartheta, \varsigma_{ij}) &= \frac{1}{2} (\lambda^A \varepsilon_{kk}^e \varepsilon_{pp}^e + 2\mu^A \varepsilon_{ij}^e \varepsilon_{ij}^e) \\ &\quad - \Lambda^A - \Omega_{ij}^A (T - T_0) \varepsilon_{ij}^e + \frac{1}{2} K^A \vartheta^2 \\ &\quad + \frac{1}{2HA} \varsigma_{ij} \varsigma_{ij} \\ M : \rho \Psi^M (\varepsilon_{ij}^e, T, \vartheta, \varsigma_{ij}) &= \frac{1}{2} (\lambda^M \varepsilon_{kk}^e \varepsilon_{pp}^e + 2\mu^M \varepsilon_{ij}^e \varepsilon_{ij}^e) \\ &\quad + \Lambda^M - \Omega_{ij}^M (T - T_0) \varepsilon_{ij}^e + \frac{1}{2} K^M \vartheta^2 \\ &\quad + \frac{1}{2HM} \varsigma_{ij} \varsigma_{ij} \end{aligned} \quad (14)$$

to austenitic and martensitic phases, respectively;  $\rho$  is the material density;  $\lambda$  and  $\mu$  are the Lamé coefficients;  $\alpha$  is a parameter that control the height of the stress–strain hysteresis loop;  $\Lambda^M$  and  $\Lambda^A$  are functions of temperature that define the phase transformation stress value;  $\Omega_{ij}$  is a tensor related to the thermal expansion coefficients;  $T_0$  is a

reference temperature in a stress-free state;  $K$  is the plastic modulus, related to isotropic hardening;  $H$  is the kinematic hardening modulus.

The use of a limited number of martensitic variants is possible due to the definition of an equivalent strain field,  $\Gamma$ , which induces phase transformations. Its definition is based on the idea that phase transformation may be induced either by volumetric or by deviatoric effects, being given by:

$$\Gamma = \frac{1}{3}\epsilon_{kk}^e + \frac{2}{3}\sqrt{3J_2^e}\text{sign}(\epsilon_{kk}^e) \tag{15}$$

The deviatoric term is defined as follows:

$$J_2^e = \frac{1}{6}\hat{\epsilon}_{ij}^e\hat{\epsilon}_{ij}^e = \frac{1}{6}\left\{(\epsilon_{11}^e - \epsilon_{22}^e)^2 + (\epsilon_{22}^e - \epsilon_{33}^e)^2 + (\epsilon_{33}^e - \epsilon_{11}^e)^2 + 6\left[(\epsilon_{12}^e)^2 + (\epsilon_{13}^e)^2 + (\epsilon_{23}^e)^2\right]\right\} \tag{16}$$

where  $\hat{\epsilon}_{ij}^e = \epsilon_{ij}^e - \frac{1}{3}\epsilon_{kk}^e\delta_{ij}$ ; and  $\delta_{ij}$  represents the Kronecker delta.

The definition of this equivalent strain field  $\Gamma$  is based on experimental observations that show that both volumetric and deviatoric effects induce phase transformations with the same qualitative behavior. Under this assumption, the equivalent field  $\Gamma$  may be interpreted as a phase transformation inductor responsible for the definition of what kind of martensitic variant is induced. For one-dimensional case,  $\Gamma = \epsilon_{11}^e$ , which reduces the model to the original one-dimensional description.

### 2.1.1 Free energy density of the mixture

After the definition of the free energy for each macroscopic phase, it is necessary to define the free energy density of the mixture, setting the volume fraction of each macroscopic phase:  $\beta^A$ , representing austenite;  $\beta^+$  and  $\beta^-$ , associated with detwinned martensites ( $M^+$  and  $M^-$ , respectively); and  $\beta^M$  associated with twinned martensite ( $M$ ). Therefore, the free energy density of the mixture is given by:

$$\begin{aligned} \rho\Psi(\epsilon_{ij}^e, T, \vartheta, \varsigma_{ij}, \beta^+, \beta^-, \beta^A, \beta^M) \\ = \rho(\beta^+\Psi^+ + \beta^-\Psi^- + \beta^A\Psi^A + \beta^M\Psi^M) \\ + I_\Theta(\beta^+, \beta^-, \beta^A, \beta^M) \end{aligned} \tag{17}$$

where  $I_\Theta(\beta^+, \beta^-, \beta^A, \beta^M)$  is the indicator function associated with the convex set  $\Theta$  [41] establishing the conditions for phases' coexistence:

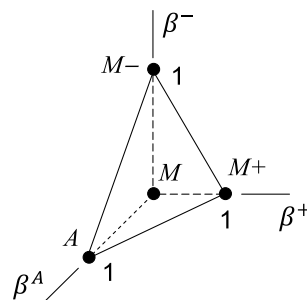


**Fig. 1** Geometrical representation of the phase's coexistence restriction

$$\Theta = \left\{ \beta^m \in \Re \mid 0 \leq \beta^m \leq 1 (m = +, -, A, M); \beta^+ + \beta^- + \beta^A + \beta^M = 1 \right\} \tag{18}$$

An indicator function is defined in such a way that it represents or indicates a specific set. Hence, an indicator function of a set  $\Theta$ ,  $I_\Theta$ , for a specific state,  $x$ , vanishes if the state belongs to the set. Otherwise, it assumes an infinite value.

In terms of the energy function, it means that there is an energy quantity that vanishes when admissible states are considered, being infinity otherwise. Lagrange multipliers constitute an equivalent approach and can replace indicator functions.

The phases' coexistence condition allows one to write  $\beta^M = 1 - \beta^+ - \beta^- - \beta^A$  in order to define the free energy density in terms of three volume fractions (instead of the four considered):

$$\begin{aligned} \rho\Psi(\epsilon_{ij}^e, T, \vartheta, \varsigma_{ij}, \beta^+, \beta^-, \beta^A) = \rho\left\{ \beta^+(\Psi^+ - \Psi^M) \right. \\ \left. + \beta^-(\Psi^- - \Psi^M) + \beta^A(\Psi^A - \Psi^M) \right. \\ \left. + \Psi^M \right\} + I_\pi \end{aligned} \tag{19}$$

Now, the indicator function  $I_\pi(\beta^+, \beta^-, \beta^A)$  is related to the convex set defined as follows, which can be geometrically interpreted by a tetrahedron in  $\beta$ -space, shown in Fig. 1.

$$\pi = \left\{ \beta^m \in \Re \mid 0 \leq \beta^m \leq 1 (m = +, -, A); \beta^+ + \beta^- + \beta^A \leq 1 \right\} \tag{20}$$

Under these assumptions, the free energy density of the mixture has the following form:

$$\begin{aligned} \rho\Psi(\varepsilon_{ij}^e, T, \vartheta, \varsigma_{ij}, \beta^+, \beta^-, \beta^A) &= \alpha\Gamma(\beta^- - \beta^+) - \Lambda(\beta^+ + \beta^-) \\ &+ \left\{ \frac{1}{2}(\lambda^A - \lambda^M)\varepsilon_{kk}^e\varepsilon_{pp}^e + (\mu^A - \mu^M)\varepsilon_{ij}^e\varepsilon_{ij}^e - (\Omega_{ij}^A - \Omega_{ij}^M)(T - T_0)\varepsilon_{ij}^e - \Lambda^{\aleph} \right. \\ &+ \frac{1}{2}(K^A - K^M)\vartheta^2 + \left. \left( \frac{1}{2H^A} - \frac{1}{2H^M} \right)\varsigma_{ij}\varsigma_{ij} \right\} \beta^A + \left\{ \frac{1}{2}\lambda^M\varepsilon_{kk}^e\varepsilon_{pp}^e + \mu^M\varepsilon_{ij}^e\varepsilon_{ij}^e \right\} \\ &- \Omega_{ij}^M(T - T_0)\varepsilon_{ij}^e + \Lambda^M + \frac{1}{2}K^M\vartheta^2 + \frac{1}{2H^M}\varsigma_{ij}\varsigma_{ij} + I_{\pi}(\beta^+, \beta^-, \beta^A) \end{aligned} \tag{21}$$

where  $\Lambda = 2\Lambda^M$  and  $\Lambda^{\aleph} = \Lambda^M + \Lambda^A$ .

An additive decomposition is now assumed by considering that the total strain,  $\varepsilon_{ij}$ , is the sum of the elastic strain,  $\varepsilon_{ij}^e$ , the plastic strain,  $\varepsilon_{ij}^p$ , and the phase transformation strain,  $\varepsilon_{ij}^t$ :

$$\varepsilon_{ij}^e = \varepsilon_{ij} - \varepsilon_{ij}^p - \varepsilon_{ij}^t \tag{22}$$

The phase transformation strain is defined as follows:

$$\varepsilon_{ij}^t = \alpha_{ijkl}^h r_{kl}(\beta^+ - \beta^-)\text{sign}(\varepsilon_{kk}^e) \tag{23}$$

where  $\alpha_{ijkl}^h$  is a fourth-order tensor related to phase transformation and its form is similar to the classical elastic tensor;  $r_{kl}$  is a second-order tensor defined from the loading history.

### 2.1.2 Thermodynamic forces

The generalized standard materials approach follows the second law of thermodynamics in order to define thermodynamic forces associated with each internal variable [12, 13, 26]:

$$\sigma_{ij} = \rho \frac{\partial \Psi}{\partial \varepsilon_{ij}^e} = \lambda \varepsilon_{kk}^e \delta_{ij} + 2\mu \varepsilon_{ij}^e + \alpha \omega_{ij}(\beta^- - \beta^+) - \Omega_{ij}(T - T_0) \tag{24}$$

$$B^+ \in -\rho \partial_{\beta^+}(\Psi) = \alpha\Gamma + \Lambda + P - \alpha_{ijkl}^h r_{kl} \Omega_{ij}(T - T_0) - \tau^+ \tag{25}$$

$$B^- \in -\rho \partial_{\beta^-}(\Psi) = -\alpha\Gamma + \Lambda + P + \alpha_{ijkl}^h r_{kl} \Omega_{ij}(T - T_0) - \tau^- \tag{26}$$

$$\begin{aligned} B^A \in -\rho \partial_{\beta^A}(\Psi) &= \Lambda^{\aleph} + P^A + \varepsilon_{ij}^e \left( \Omega_{ij}^A - \Omega_{ij}^M \right) (T - T_0) \\ &- \frac{1}{2}(K^A - K^M)\vartheta^2 - \left( \frac{1}{2H^A} - \frac{1}{2H^M} \right)\varsigma_{ij}\varsigma_{ij} - \tau^A \end{aligned} \tag{27}$$

$$\begin{aligned} X_{ij} = -\rho \frac{\partial \Psi}{\partial \varepsilon_{ij}^p} &= \lambda \varepsilon_{kk}^e \delta_{ij} + 2\mu \varepsilon_{ij}^e \\ &+ \alpha \omega_{ij}(\beta^- - \beta^+) - \Omega_{ij}(T - T_0) = \sigma_{ij} \end{aligned} \tag{28}$$

$$Y \in -\rho \frac{\partial \Psi}{\partial \vartheta} = -K\vartheta \tag{29}$$

$$Z_{ij} \in -\rho \frac{\partial \Psi}{\partial \varsigma_{ij}} = -\frac{1}{H} \varsigma_{ij} \tag{30}$$

where  $B^+, B^-, B^A, R_{ij}, X_{ij}, Y$  and  $Z_{ij}$  are thermodynamic forces associated with state variables;  $\sigma_{ij}$  is the stress tensor;  $\tau$  is related to the sub-differential with respect to volume fractions being associated with projections in the  $\beta$ -space (Fig. 1).

$$\tau = (\tau^+, \tau^-, \tau^A) \in \partial I_{\pi}(\beta^+, \beta^-, \beta^A) \tag{31}$$

Moreover, auxiliary quantities are defined as follows:

$$\omega_{ij} = \frac{1}{3} \delta_{ij} + \left[ \frac{3\varepsilon_{ij}^e - \varepsilon_{kk}^e \delta_{ij}}{3\sqrt{3}J_2^e} \right] \text{sign}(\varepsilon_{kk}^e) \tag{32}$$

$$\begin{aligned} P &= \left( \lambda \varepsilon_{mm}^e \alpha_{ijkl}^h r_{kl} \delta_{ij} + 2\mu \varepsilon_{ij}^e \alpha_{ijkl}^h r_{kl} \right) \\ &+ \alpha(\beta^- - \beta^+) \left\{ \frac{1}{3} \alpha_{ijkl}^h r_{kl} \delta_{ij} + \frac{2P^{\alpha}}{\sqrt{3}J_2^e} \text{sign}(\varepsilon_{kk}^e) \right\} \end{aligned} \tag{33}$$

$$P^A = -\frac{1}{2} \left( \lambda^A \varepsilon_{kk}^e \varepsilon_{pp}^e + 2\mu^A \varepsilon_{ij}^e \varepsilon_{ij}^e \right) + \frac{1}{2} \left( \lambda^M \varepsilon_{kk}^e \varepsilon_{pp}^e + 2\mu^M \varepsilon_{ij}^e \varepsilon_{ij}^e \right) \tag{34}$$

$$\begin{aligned} P^{\alpha} &= \frac{\alpha_S^h}{6} \{ (r_{11} - r_{22})(\varepsilon_{11}^e - \varepsilon_{22}^e) + (r_{22} - r_{33})(\varepsilon_{22}^e - \varepsilon_{33}^e) \\ &+ (r_{33} - r_{11})(\varepsilon_{33}^e - \varepsilon_{11}^e) + 6(r_{12}\varepsilon_{12}^e + r_{13}\varepsilon_{13}^e + r_{23}\varepsilon_{23}^e) \} \end{aligned} \tag{35}$$

Based on the presented equations, the material parameters are defined by a rule of mixtures of each one of the phase properties:

$$\lambda = \lambda^M + \beta^A(\lambda^A - \lambda^M) \tag{36}$$

$$\mu = \mu^M + \beta^A(\mu^A - \mu^M) \tag{37}$$

$$\Omega_{ij} = \Omega_{ij}^M + \beta^A(\Omega_{ij}^A - \Omega_{ij}^M) \tag{38}$$

$$K = K^M + \beta^A (K^A - K^M) \tag{39}$$

$$\frac{1}{H} = \frac{1}{H^M} + \beta^A \left( \frac{1}{H^A} - \frac{1}{H^M} \right) \tag{40}$$

and, since  $\lambda \varepsilon_{mm}^e \delta_{ij} + 2\mu \varepsilon_{ij}^e = E_{ijkl} \varepsilon_{kl}^e$ , it is possible to rewrite the stress equation as follows:

$$\sigma_{ij} = E_{ijkl} \varepsilon_{kl}^e + \alpha \omega_{ij} (\beta^- - \beta^+) - \Omega_{ij} (T - T_0) \tag{41}$$

where  $E_{ijkl} = E_{ijkl}^M + \beta^A (E_{ijkl}^A - E_{ijkl}^M)$  refers to the elastic tensor. Note that Lamé coefficients,  $\lambda$  and  $\mu$ , can be expressed in terms of the engineering constants as follows:

$$\lambda = \frac{\nu E}{(1 + \nu)(1 - 2\nu)} \quad \text{and} \quad G = \mu = \frac{E}{2(1 + \nu)} \tag{42}$$

where  $E$  is the elastic modulus,  $G$  is the shear modulus and  $\nu$  is the Poisson’s ratio.

### 2.2 Pseudo-potential of dissipation

The thermomechanical behavior of SMAs is intrinsically dissipative and therefore, it is important to establish the pseudo-potential of dissipation that allows the description of dissipation processes. It is assumed that this potential may be split into mechanical,  $\Phi^M$ , and thermal,  $\Phi^H$ , parts:

$$\begin{aligned} \Phi(\dot{\beta}^+, \dot{\beta}^-, \dot{\beta}^A, \dot{\varepsilon}_{ij}^p, \dot{\vartheta}, \dot{\zeta}_{ij}, q) \\ = \Phi^M(\dot{\beta}^+, \dot{\beta}^-, \dot{\beta}^A, \dot{\varepsilon}_{ij}^p, \dot{\vartheta}, \dot{\zeta}_{ij}) + \Phi^H(q) \end{aligned} \tag{43}$$

Since the description of the thermomechanical couplings is beyond the scope of this paper, only the mechanical part is of concern. Using the dual of the pseudo-potential of dissipation, its mechanical part can be expressed as a function of thermodynamic forces by the following equation:

$$\begin{aligned} \bar{\Phi}^M(B^+, B^-, B^A, X_{ij}, Y, Z_{ij}) = & \frac{1}{2\eta} (B^+ + \eta^I Y + \eta_{ij}^K Z_{ij})^2 \\ & + \frac{1}{2\eta} (B^- + \eta^I Y + \eta_{ij}^K Z_{ij})^2 \\ & + \frac{1}{2\eta^A} (B^A - \eta^I Y - \eta_{ij}^K Z_{ij})^2 \\ & + I_\chi(B^+, B^-, B^A) + I_f(X_{ij}, Y, Z_{ij}) \end{aligned} \tag{44}$$

The generalized standard materials approach is adopted to define the thermodynamic fluxes as follows [12, 13, 26]:

$$\begin{aligned} \dot{\beta}^+ \in \partial_{B^+}(\bar{\Phi}^M) = & \frac{B^+}{\eta} + \frac{\eta^I}{\eta} Y + \frac{\eta_{ij}^K}{\eta} Z_{ij} + \Upsilon^+ \\ = & \frac{B^+}{\eta} - \frac{\eta^I}{\eta} K \vartheta - \frac{\eta_{ij}^K}{\eta} \frac{\zeta_{ij}}{H} + \Upsilon^+ \end{aligned} \tag{45}$$

$$\begin{aligned} \dot{\beta}^- \in \partial_{B^-}(\bar{\Phi}^M) = & \frac{B^-}{\eta} + \frac{\eta^I}{\eta} Y + \frac{\eta_{ij}^K}{\eta} Z_{ij} + \Upsilon^- \\ = & \frac{B^-}{\eta} - \frac{\eta^I}{\eta} K \vartheta - \frac{\eta_{ij}^K}{\eta} \frac{\zeta_{ij}}{H} + \Upsilon^- \end{aligned} \tag{46}$$

$$\begin{aligned} \dot{\beta}^A \in \partial_{B^A}(\bar{\Phi}^M) = & \frac{B^A}{\eta^A} + \frac{\eta^I}{\eta^A} Y + \frac{\eta_{ij}^K}{\eta^A} Z_{ij} + \Upsilon^A \\ = & \frac{B^A}{\eta^A} - \frac{\eta^I}{\eta^A} K \vartheta - \frac{\eta_{ij}^K}{\eta^A} \frac{\zeta_{ij}}{H} + \Upsilon^A \end{aligned} \tag{47}$$

$$\dot{\varepsilon}_{ij}^p \in \partial_{X_{ij}}(\bar{\Phi}^M) = \gamma \frac{\hat{\sigma}_{ij} - \zeta_{ij}}{\|\hat{\sigma}_{ij} - \zeta_{ij}\|} \tag{48}$$

$$\begin{aligned} \dot{\vartheta} \in \partial_Y(\bar{\Phi}^M) = & \sqrt{\frac{2}{3}} \gamma + \eta^I (\dot{\beta}^+ + \dot{\beta}^- + \dot{\beta}^A) \\ = & \sqrt{\frac{2}{3}} |\dot{\varepsilon}_{ij}^p| + \eta^I (\dot{\beta}^+ + \dot{\beta}^- + \dot{\beta}^A) \end{aligned} \tag{49}$$

$$\begin{aligned} \dot{\zeta}_{ij} \in \partial_{Z_{ij}}(\bar{\Phi}^M) = & \frac{2}{3} \gamma H \frac{\hat{\sigma}_{ij} - \zeta_{ij}}{\|\hat{\sigma}_{ij} - \zeta_{ij}\|} + \eta_{ij}^K (\dot{\beta}^+ + \dot{\beta}^- + \dot{\beta}^A) \\ = & \frac{2}{3} H \dot{\varepsilon}_{ij}^p + \eta_{ij}^K (\dot{\beta}^+ + \dot{\beta}^- + \dot{\beta}^A) \end{aligned} \tag{50}$$

where  $\hat{\sigma}_{ij} = \sigma_{ij} - \frac{1}{3} \sigma_{kk} \delta_{ij}$  is the deviatoric tensor and  $\|\hat{\sigma}_{ij} - \zeta_{ij}\|$  is the euclidean norm of  $\hat{\sigma}_{ij} - \zeta_{ij}$ , defined as follows,

$$\|\hat{\sigma}_{ij} - \zeta_{ij}\| = \sqrt{(\hat{\sigma}_{ij} - \zeta_{ij})(\hat{\sigma}_{ij} - \zeta_{ij})} \tag{51}$$

It should be pointed out that  $\eta$  and  $\eta^A$  are associated with the internal dissipation of each material phase. Besides,  $\eta^I$  defines the coupling between phase transformations and the isotropic hardening. The coupling between phase transformations and the kinematic hardening is defined by the second-order tensor  $\eta_{ij}^K$ .  $\Upsilon$  is related to the sub-differential with respect to  $\dot{\beta}^+$ ,  $\dot{\beta}^-$  and  $\dot{\beta}^A$ .

$$\Upsilon = (\Upsilon^+, \Upsilon^-, \Upsilon^A) \in \partial I_\chi(\dot{\beta}^+, \dot{\beta}^-, \dot{\beta}^A) \tag{52}$$

where  $I_\chi$  is an indicator function of the convex set  $\chi$  that defines restrictions associated with the phase transformations. Physically, these restrictions establish conditions for internal sub-loops due to incomplete phase transformations and also avoid improper phase transformations [47]. The definition of this convex set needs to consider an equivalent stress field, similar to the strain field, given by:



$$\Gamma^\sigma = \frac{1}{3}\sigma_{kk} + \frac{2}{3}\sqrt{3J_2^\sigma} \text{sign}(\sigma_{kk}) \tag{53}$$

Besides, it is important to define the quantities at the initial state:

$$\varepsilon_{ij}^e(0) = \varepsilon_{ij}^e - \frac{\Omega_{ij}}{E_{ijkl}} \tag{54}$$

$$\Gamma_0 = \frac{1}{3}\varepsilon_{kk}^e(0) + \frac{2}{3}\sqrt{3J_2^\sigma(0)} \text{sign}(\varepsilon_{kk}^e(0)) \tag{55}$$

The convex set  $\chi$  is now defined by considering two different situations associated with mechanical and thermal loadings. Basically, when mechanical loadings govern phase transformations,  $\dot{\Gamma}^\sigma \neq 0$ , the convex set is given by:

$$\chi = \left\{ \dot{\beta}^n \in \Re \left| \begin{array}{l} \dot{\Gamma} \dot{\beta}^+ \geq 0; \dot{\Gamma} \dot{\beta}^A \leq 0 \text{ if } \Gamma_0 > 0 \\ \dot{\Gamma} \dot{\beta}^- \leq 0; \dot{\Gamma} \dot{\beta}^A \geq 0 \text{ if } \Gamma_0 < 0 \end{array} \right. \right\} \tag{56}$$

On the other hand, when thermal loadings govern phase transformation,  $\dot{\Gamma}^\sigma = 0$ , the convex set  $\chi$  is defined as follows, by considering three subsets ( $\chi_1, \chi_2, \chi_3$ ):

$$\chi_1 = \left\{ \dot{\beta}^n \in \Re \left| \dot{\Gamma} \dot{\beta}^A \geq 0 \right. \right\} \tag{57a}$$

$$\chi_2 = \left\{ \dot{\beta}^n \in \Re \left| \dot{\Gamma} \dot{\beta}^+ = 0 \left[ \begin{array}{l} \text{if } \dot{T} > 0, \dot{\beta}^+ > 0 \text{ and } \beta_s^+ \neq 0 \\ \text{if } \dot{T} > 0, \beta^+ \neq \beta_s^+ \text{ and } \beta_s^+ = 0 \\ \text{if } \dot{T} > 0, \dot{\beta}^A = 0 \\ \text{if } \dot{T} < 0, \Gamma^\sigma = 0 \text{ and } \beta^+ \neq \beta_s^+ \end{array} \right. \right. \right\} \tag{57b}$$

$$\chi_3 = \left\{ \dot{\beta}^n \in \Re \left| \dot{\Gamma} \dot{\beta}^- = 0 \left[ \begin{array}{l} \text{if } \dot{T} > 0, \dot{\beta}^- > 0 \text{ and } \beta_s^- \neq 0 \\ \text{if } \dot{T} > 0, \beta^- \neq \beta_s^- \text{ and } \beta_s^- = 0 \\ \text{if } \dot{T} > 0, \dot{\beta}^A = 0 \\ \text{if } \dot{T} < 0, \Gamma^\sigma = 0 \text{ and } \beta^- \neq \beta_s^- \end{array} \right. \right. \right\} \tag{57c}$$

where  $\beta_s^+$  and  $\beta_s^-$  are the values of  $\beta^+$  and  $\beta^-$ , respectively, when the phase transformation begins to take place.

Plastic behavior is described using the classical approach considering that  $\gamma$  is the plastic multiplier and  $I_f$  is the indicator function related to the classical plasticity;  $f$  is defined from the characteristics of the yield surface as follows [54].

$$f = \|\hat{\sigma}_{ij} - \varsigma_{ij}\| - \sqrt{\frac{2}{3}}(\sigma_Y - K\vartheta) \tag{58}$$

where  $\sigma_Y$  is the yield stress. Plastic behavior is subjected to the Kuhn–Tucker conditions,

$$\gamma \geq 0, \quad f \leq 0 \quad \text{and} \quad \gamma f = 0 \tag{59}$$

and the consistency condition, when  $f = 0$ ,

$$\gamma \dot{f} = 0. \tag{60}$$

### 2.3 Constitutive equations

The standard generalized material approach establishes a set of constitutive equations that describes the SMA thermomechanical behavior satisfying the second law of thermodynamics [12, 13, 26]. This set is summarized in Box 1.

It should be highlighted some aspects of the phase transformation process. On the one hand, if  $\Gamma \geq 0$  the variant  $M^+$  is induced, increasing the value of  $\beta^+$ . On the other hand, the variant  $M^-$  is induced when  $\Gamma < 0$ , increasing the value of  $\beta^-$ . Moreover, it should be pointed out that shear behavior has a neutral influence on the martensitic phase induction since the sign of shear strains does not appear in the inductor  $\Gamma$ . Therefore, this induction tends to follow the volumetric expansion sign.

The model parameters are related to different aspects, including thermo-elasto- plasticity and phase transformation parameters. Classical thermo-elastic parameters are:  $E_{ijkl}^A, E_{ijkl}^M, \Omega_{ij}^A, \Omega_{ij}^M$ . Plastic parameters are basically related to

#### Box 1 Constitutive equations

---


$$\begin{aligned} \sigma_{ij} &= E_{ijkl} \varepsilon_{kl}^e + \alpha \omega_{ij} (\beta^- - \beta^+) - \Omega_{ij} (T - T_0) \\ \dot{\beta}^+ &= \frac{1}{\eta} \left\{ \alpha \Gamma + \Lambda + P - \alpha_{ijkl}^h r_{kl} \Omega_{ij} (T - T_0) - \eta^l K \vartheta - \eta_{ij}^K \frac{\varsigma_{ij}}{H} - \tau^+ \right\} + \Upsilon^+ \\ \dot{\beta}^- &= \frac{1}{\eta} \left\{ -\alpha \Gamma + \Lambda - P + \alpha_{ijkl}^h r_{kl} \Omega_{ij} (T - T_0) - \eta^l K \vartheta - \eta_{ij}^K \frac{\varsigma_{ij}}{H} - \tau^- \right\} + \Upsilon^- \\ \dot{\beta}^A &= \frac{1}{\eta^A} \left\{ P^A + \Lambda^N + \varepsilon_{ij}^e (\Omega_{ij}^A - \Omega_{ij}^M) (T - T_0) - \frac{1}{2} (K^A - K^M) \vartheta^2 - \left( \frac{1}{2H^A} - \frac{1}{2H^M} \right) \varsigma_{ij} \varsigma_{ij} + \eta^l K \vartheta + \eta_{ij}^K \frac{\varsigma_{ij}}{H} - \tau^A \right\} + \Upsilon^A \\ \dot{\varepsilon}_{ij}^p &= \gamma \frac{\hat{\sigma}_{ij} - \varsigma_{ij}}{\hat{\sigma}_{ij} - \varsigma_{ij}} \\ \dot{\vartheta} &= \sqrt{\frac{2}{3}} \gamma + \eta^l (\dot{\beta}^+ + \dot{\beta}^- + \dot{\beta}^A) \\ \dot{\varsigma}_{ij} &= \frac{2}{3} H \dot{\varepsilon}_{ij}^p + \eta_{ij}^K (\dot{\beta}^+ + \dot{\beta}^- + \dot{\beta}^A) \end{aligned}$$

Yield surface and its conditions

$$\begin{aligned} f &= \hat{\sigma}_{ij} - \varsigma_{ij} - \sqrt{\frac{2}{3}}(\sigma_Y - K\vartheta) \\ \gamma &\geq 0, \quad f \leq 0 \quad \text{and} \quad \gamma f = 0 \\ \gamma \dot{f} &= 0 \text{ if } f = 0 \end{aligned}$$


---

yield surface definition considering yield stress, kinematic and isotropic hardening:  $\sigma_Y^A, \sigma_Y^M, K^A, K^M, H^A, H^M$ . Besides, phase transformation parameters consider the horizontal and vertical size of the hysteresis loop, critical phase transformation stress values and dissipation aspects of the hysteresis:  $\alpha, \alpha_{ijkl}^h, \Lambda, \Lambda^N, \eta, \eta^A$ . Moreover, there are parameters related to plastic-phase transformation coupling:  $\eta^l$  and  $\eta_{ij}^K$ .

The coupling of the phase transformations with the kinematic hardening is represented by the second-order tensor  $\eta_{ij}^K$  defined as follows:

$$\eta_{ij}^K = \eta^K \begin{bmatrix} 1 & 1 & 1 \\ 1 & 1 & 1 \\ 1 & 1 & 1 \end{bmatrix} \tag{61}$$

It is important to highlight that some constants are split due to temperature or loading dependence. In this regard, some changes can be used to facilitate adjustments with experimental data. Tensor quantities consider the same form of the classical isotropic elastic tensor. Hence, normal and shear behaviors are characterized in different ways. In this regard, it is necessary to show the details of some parameters, which is done in the forthcoming definitions.

The parameter  $\alpha_{ijkl}^h$  is a fourth-order tensor related to phase transformations that considers different parameters for normal,  $\alpha_N^h$ , and shear,  $\alpha_S^h$ , behaviors. Its form is similar to the classical isotropic elastic tensor given by,

$$\alpha_{ijkl}^h \equiv \begin{bmatrix} \alpha_N^h & \alpha_N^h - \alpha_S^h & \alpha_N^h - \alpha_S^h & 0 & 0 & 0 \\ \alpha_N^h - \alpha_S^h & \alpha_N^h & \alpha_N^h - \alpha_S^h & 0 & 0 & 0 \\ \alpha_N^h - \alpha_S^h & \alpha_N^h - \alpha_S^h & \alpha_N^h & 0 & 0 & 0 \\ 0 & 0 & 0 & \alpha_S^h & 0 & 0 \\ 0 & 0 & 0 & 0 & \alpha_S^h & 0 \\ 0 & 0 & 0 & 0 & 0 & \alpha_S^h \end{bmatrix} \tag{62}$$

The definition of transformation strain,  $\varepsilon_{ij}^t$ , needs the definition of parameter  $r_{kl}$  that is a symmetric second-order tensor related to the loading history as follows:

$$r_{kl} = \begin{cases} +1, & \text{if } \sigma_{kl} > 0 \\ 0, & \text{if } \sigma_{kl} = 0 \\ -1, & \text{if } \sigma_{kl} < 0 \end{cases} \tag{63}$$

For situations where mechanical loadings are provided by multiaxial, non-simultaneous load history, tensor  $r_{kl}$  is evaluated as follows for the subsequent loadings:

$$r_{kl} = \frac{\sigma_{kl}}{|S_{kl}^{\max}|}, \quad \text{if } \beta^+ \neq 0 \text{ or } \beta^- \neq 0 \tag{64}$$

Temperature-dependent functions  $\Lambda = \Lambda(T)$  and  $\Lambda^N = \Lambda^N(T)$  define the phase transformation stress level as follows:

$$\Lambda = 2\Lambda^M = \begin{cases} -\bar{L} + \frac{L}{T^M}(T - T^M), & \text{if } T > T^M \\ -\bar{L}, & \text{if } T \leq T^M \end{cases} \tag{65}$$

$$\Lambda^N = \Lambda^M + \Lambda^A = \begin{cases} -\bar{L}^A + \frac{L^A}{T^M}(T - T^M), & \text{if } T > T^M \\ -\bar{L}^A, & \text{if } T \leq T^M \end{cases} \tag{66}$$

where  $T^M$  is the temperature below which the martensitic phase becomes stable. Note that the phase transformation stress level is constant for  $T < T^M$ .

Parameters  $\bar{L}, L, \bar{L}^A$  and  $L^A$  are related to phase transformation critical stresses. In order to consider different levels of phase transformation stress for normal and shear behaviors, each one of them may be expressed by a fourth-order tensor that defines normal and shear properties, following the same structure of the parameter  $\alpha_{ijkl}^h$ . In this regard,  $L$  represents the general form of each one of these parameters. The others are defined in analogous way.

$$\begin{cases} L = r_{ij}\tilde{L}_{ijkl}r_{kl}, & \text{if } \Gamma^\sigma \neq 0 \\ L = L_N, & \text{otherwise} \end{cases} \tag{67}$$

where

$$\tilde{L}_{ijkl} = \begin{bmatrix} L_N & L_N - L_S & L_N - L_S & 0 & 0 & 0 \\ L_N - L_S & L_N & L_N - L_S & 0 & 0 & 0 \\ L_N - L_S & L_N - L_S & L_N & 0 & 0 & 0 \\ 0 & 0 & 0 & 2L_S & 0 & 0 \\ 0 & 0 & 0 & 0 & 2L_S & 0 \\ 0 & 0 & 0 & 0 & 0 & 2L_S \end{bmatrix} \tag{68}$$

where  $L_N$  and  $L_S$  respectively represents the normal and the shear components.

The phase transformation dissipation can be defined contemplating different characteristics of the phase transformation kinetics during loading and unloading processes. Therefore, different values can be employed for the parameters  $\eta$  and  $\eta^A$ , in the following form

$$\begin{cases} \eta = \eta_L, & \text{if } \dot{\Gamma} > 0 \\ \eta = \eta_U, & \text{if } \dot{\Gamma} < 0 \end{cases}; \quad \begin{cases} \eta^A = \eta_L^A, & \text{if } \dot{\Gamma} > 0 \\ \eta^A = \eta_U^A, & \text{if } \dot{\Gamma} < 0 \end{cases} \tag{69}$$

where parameters  $\eta_L, \eta_U, \eta_L^A$  and  $\eta_U^A$  are calculated considering fourth-order tensors, in the same way of the Eqs. (67) and (68).

Concerning plastic effects, the yield surface is defined by the yield stress,  $\sigma_Y$ , that has different values for the austenitic and martensitic phases. Their values are also temperature dependent tending to decrease for high temperatures. Different expressions can be employed for the proper description of these conditions. Here, for the sake of simplicity, temperature variation is assumed to be:

$$\begin{cases} \sigma_Y = \sigma_Y^M, & \text{if } T \leq T^M \\ \sigma_Y = \frac{\sigma_Y^M(T^A - T) + \sigma_Y^{Ai}(T - T^M)}{T^A - T^M}, & \text{if } T^M < T \leq T^A \\ \sigma_Y = \frac{\sigma_Y^{Ai}(T^F - T) + \sigma_Y^Af(T - T^A)}{T^F - T^A}, & \text{if } T^M < T \leq T^F \end{cases} \tag{70}$$

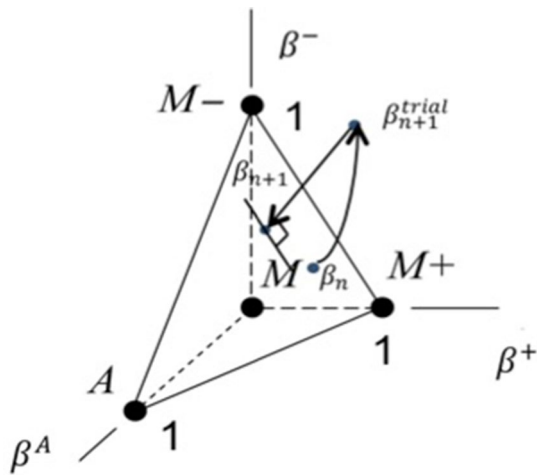


**Fig. 2** Projection algorithm for phase transformation

where  $T^A$  is the temperature above with the austenitic phase is stable and  $T^F$  is a reference temperature for the determination of the yield stress for high temperatures;  $\sigma_Y^{Ai}$  and  $\sigma_Y^{Af}$  define the thermal variation of the yield stress of the austenitic phase.

Under these assumptions, the following parameters are employed to defined the yield surface, instead of  $\sigma_Y$ :  $\sigma_Y^M$ ,  $\sigma_Y^{Ai}$ ,  $\sigma_Y^{Af}$ ,  $T^F$ ,  $T^A$ . Besides, a single parameter,  $\eta^K$  is used instead of the tensor quantity  $\eta_{ij}^K$ . Phase transformation tensor  $\alpha_{ijkl}^h$  considers different parameters for normal and shear behaviors:  $\alpha_N^h$  and  $\alpha_S^h$ . The definition of phase transformation stress levels,  $\Lambda$  and  $\Lambda^S$ , employs the following parameters:  $\bar{L}_N$ ,  $\bar{L}_S$ ,  $L_N$ ,  $L_S$ ,  $\bar{L}_N^A$ ,  $\bar{L}_S^A$ ,  $L_N^A$ ,  $L_S^A$ , and  $T^M$ . The same approach is adopted for the dissipation aspects of the phase transformation  $\eta$  and  $\eta^A$ .

The model parameters can be adjusted from tensile tests at different temperatures. DSC (differential scanning calorimetry) tests can employed to define phase transformation temperatures. An important point related to the model is its flexibility that allows the description of several thermomechanical behaviors of SMAs, using the same set of parameters.

### 3 Numerical procedure

In order to deal with the nonlinearities of the formulation, the solution of the constitutive equations employs the operator split technique [36] associated with an iterative procedure. Under this assumption, the coupled equations are solved as sets of uncoupled problems. In this section, first, the numerical procedure for the phase transformation is presented and afterwards, the procedure associated with plastic behavior is of concern.

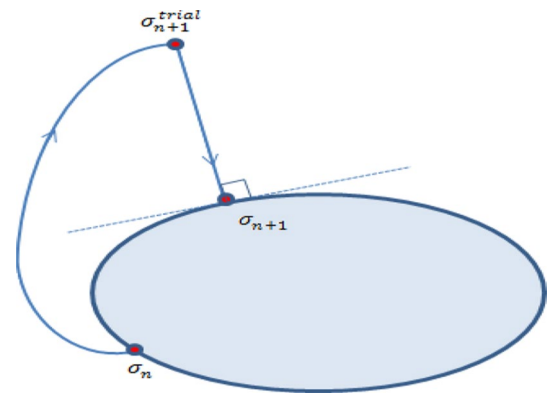


**Fig. 3** Return-mapping algorithm [54]

Basically, it is assumed that there are mechanical and thermal driving variables for simulations. Mechanical loadings may be stress or strain driving cases; thermal loadings are related to temperature driving case. Therefore, a numerical simulation implies the knowledge of the stress or strain history and also the temperature history.

#### 3.1 Phase transformation procedure

Phase transformation problem is treated by assuming the operator split technique, defining a predictor–corrector approach. The predictor step assumes that phase transformation does not occur, defining a trial state where volume fractions are identical to the previous state. Mathematically speaking, this procedure implies to neglect the sub-differentials. Therefore, the Euler implicit method is employed to calculate the volume fractions ( $\beta^+$ ,  $\beta^-$ ,  $\beta^A$ ). If the trial state obeys the constraints represented by the convex sets  $\pi$  and  $\chi$ , then it is the actual state. Otherwise, the sub-differentials need to be calculated by orthogonal projections to the boundary of the domain represented by both sets. Under this assumption, sub-differentials of the convex sets can be understood as projections. Another interpretation is to replace sub-differentials by Lagrange multipliers. The projection related to the convex set  $\pi$  is based on the nearest point of the surface of the tetrahedron of Fig. 2, being calculated step by step, according to the constraints imposed by the indicator function  $I_\pi$ . The projection assures that the calculated volume fractions obey the internal restrictions imposed by the model [44]. An iterative numerical procedure assures that this approach converges.

#### 3.2 Plasticity procedure

The elasto-plastic numerical approach considers the classical return-mapping algorithm [54]. The general idea

is similar to the one employed for phase transformation problem. Initially, it is assumed a trial state where plastic strains do not occur. Then, constraints related to yield surface are analyzed. Return mapping algorithm is employed to perform the projection from the trial to actual state, using a orthogonal projection to the yield surface.

The plastic flow is governed by the following equations:

$$\dot{\varepsilon}_{ij}^p = \gamma \varphi_{ij} \tag{71}$$

$$\dot{\zeta}_{ij} = \gamma \frac{2}{3} H \varphi_{ij} \tag{72}$$

$$\dot{\nu} = \gamma \sqrt{\frac{2}{3}} \tag{73}$$

where  $\varphi_{ij}$  is the normal unit vector of the Von Mises yield surface, defined as follows

$$\varphi_{ij} = \frac{\zeta_{ij}}{\|\zeta_{ij}\|} = \frac{\partial f(\sigma_{ij}, \varsigma_{ij})}{\partial \sigma_{ij}} \tag{74}$$

where  $\zeta_{ij} = \hat{\sigma}_{ij} - \varsigma_{ij}$ .

The implicit Euler method is employed to discretize the equations. The trial state is defined by assuming that no plastic strain occur:

$$f_{n+1}^{\text{trial}} = \left\| \left( \zeta_{ij}^{\text{trial}} \right)_{n+1} \right\| - \sqrt{\frac{2}{3}} (\sigma_Y - K \nu_n) \tag{75}$$

If the trial state is admissible, then  $f_{n+1}^{\text{trial}} \leq 0$ , and the trial state is the actual one. Otherwise, the trial state is not admissible,  $f_{n+1}^{\text{trial}} > 0$ , and the Kuhn–Tucker conditions are violated. Therefore, it is necessary to calculate the actual state using the return mapping algorithm. This is the correction step, performed using the plastic multiplier,  $\Delta\gamma$ , that establishes the projection in the yield surface where  $f_{n+1} = 0$ . Figure 3 presents the projection from the trial to the actual state, which calculation is presented in the sequence.

$$\Delta\gamma = \frac{f_{n+1}^{\text{trial}}}{2\mu + \frac{2}{3}(H + K)} \tag{76}$$

### 4 Numerical simulations: uniaxial tests

The objective of this section is to evaluate the capability of the proposed model to describe the thermomechanical behavior of one-dimensional SMA media. Typical behaviors are treated, including pseudoelasticity and shape

**Table 1** Model parameters based on experimental tests due to Tobushi et al. [60]

$E^A$ (GPa)	$E^M$ (GPa)	$\Omega^A$ (MPa/K)	$\Omega^M$ (MPa/K)	$\alpha_N^h$ (MPa)	$\alpha_S^h$ (MPa)
54	42	0.74	0.17	0.0473	0.02
$\alpha$ (MPa)	$\bar{L}_N$ (MPa)	$L_N$ (MPa)	$\bar{L}_N^A$ (MPa)	$L_N^A$ (MPa)	$\bar{L}_S$ (MPa)
330	0.15	41.5	0.63	185	0.15
$L_S$ (MPa)	$\bar{L}_S^A$ (MPa)	$L_S^A$ (MPa)	$T^M$ (K)	$T^F$ (K)	$\sigma_Y^M$ (GPa)
41.5	0.63	185	291.4	423	0.5
$\sigma_Y^{Ai}$ (GPa)	$\sigma_Y^{Af}$ (GPa)	$K^A$ (GPa)	$K^M$ (GPa)	$H^A$ (GPa)	$H^M$ (GPa)
1.5	1	1.4	0.4	4	1.1
$\eta^I$	$\eta^K$	$(\eta_L)_N$ (MPa s)	$(\eta_U)_N$ (MPa s)	$(\eta_L^A)_N$ (MPa s)	$(\eta_U^A)_N$ (MPa s)
−0.01	−0.01	1	2.7	1	2.7
$(\eta_L)_S$ (MPa s)	$(\eta_U)_S$ (MPa s)	$(\eta_U^A)_S$ (MPa s)	$(\eta_U^A)_S$ (MPa s)	$\nu^A$	$\nu^M$
1	2.7	1	2.7	0	0

**Fig. 4** Pseudoelastic behavior based on testes from Tobushi et al. [60]. Numerical-experimental comparison for  $T = 373$  K and  $T = 353$  K

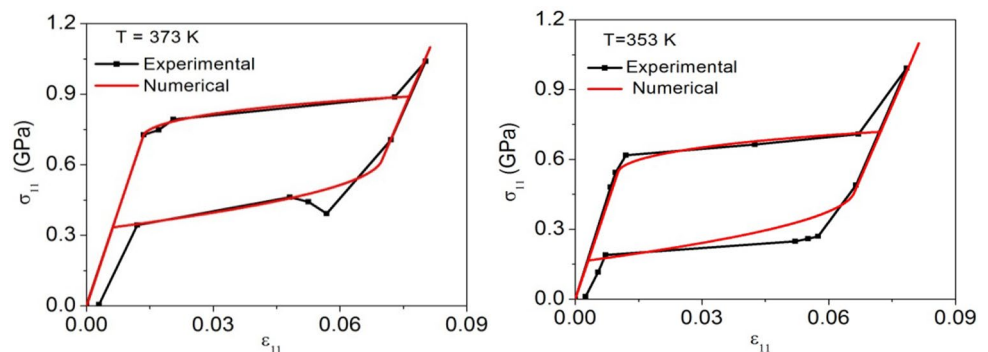
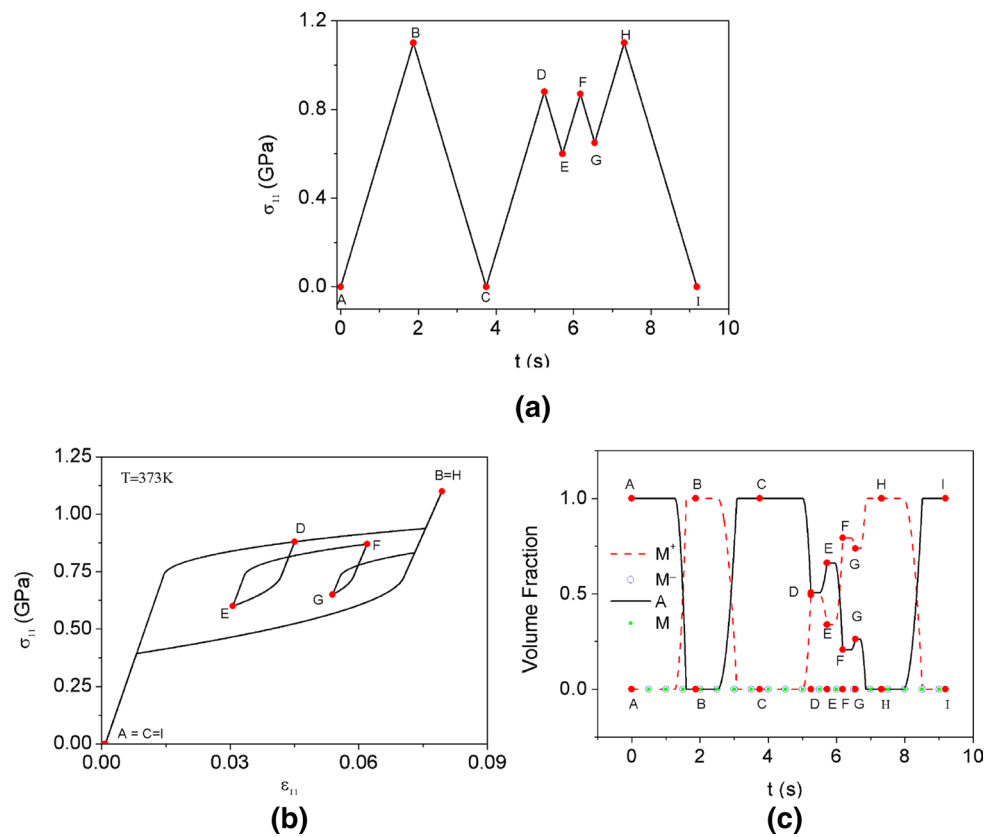


**Fig. 5** Pseudoelastic behavior with internal subloops. **a** Cyclic stress loading; **b** stress–strain curve; **c** volume fraction evolution



memory effect. Stress driving simulations are carried out. Table 1 presents the parameters employed for the numerical simulations. These parameters are adjusted based on experimental results due to Tobushi et al. [60] that consider pseudoelastic tests of SMA wires at different temperatures. This adjustment considers classical parameter values for the thermo-elasto-plastic behavior. Besides, phase transformation temperatures are defined from DSC tests and it is assumed  $T_0 = 307$  K. Poisson ratio vanishes for the uniaxial tests. It should be highlighted that all tests are carried out with the same set of parameters, showing the flexibility of the model to represent distinct thermomechanical phenomena of SMAs.

Numerical simulations are now performed for pseudoelastic tests. Figure 4 presents a comparison between numerical and experimental data performed at two different temperatures [60]:  $T = 373$  K and  $T = 353$  K. Note that numerical results capture the general behavior of SMAs, showing a good agreement with experimental data, that includes the hysteresis loop and its change due to temperature variation.

The forthcoming analyses consider qualitative verifications related to the proposed model. The idea is to use the same set of parameters to evaluate the model capability to describe typical thermomechanical behaviors of SMAs.

Internal sub-loops due to incomplete phase transformations; shape memory effect; temperature-induced phase transformations; and plasticity are carried out for uniaxial tests. In general, these results are previously addressed using one-dimensional model showing the agreement with experimental data. Here, results are obtained from the three-dimensional model, showing that it is able to reproduce the general behaviors of SMAs.

#### 4.1 Internal sub-loops due to incomplete phase transformations

A pseudoelastic behavior is now in focus by imposing a cyclic stress loading process shown in Fig. 5a together with a constant temperature. Under this loading process, a complete phase transformation cycle is performed followed by incomplete phase transformation cycles, as can be observed in Fig. 5b, c, presented as stress–strain curve and volume fraction time evolution, respectively. It should be pointed out the general aspect of the minor loops that occur inside major loops. Each minor loop is an internal subloop that has an elastic response during loading process and another one during unloading, meaning that volume fractions remain constant. Initially, the SMA sample is in austenitic phase, being subjected

**Fig. 6** Shape memory effect. **a** Stress loading history; **b** thermal loading history; **c** stress–strain–temperature curve; **d** volume fraction evolution

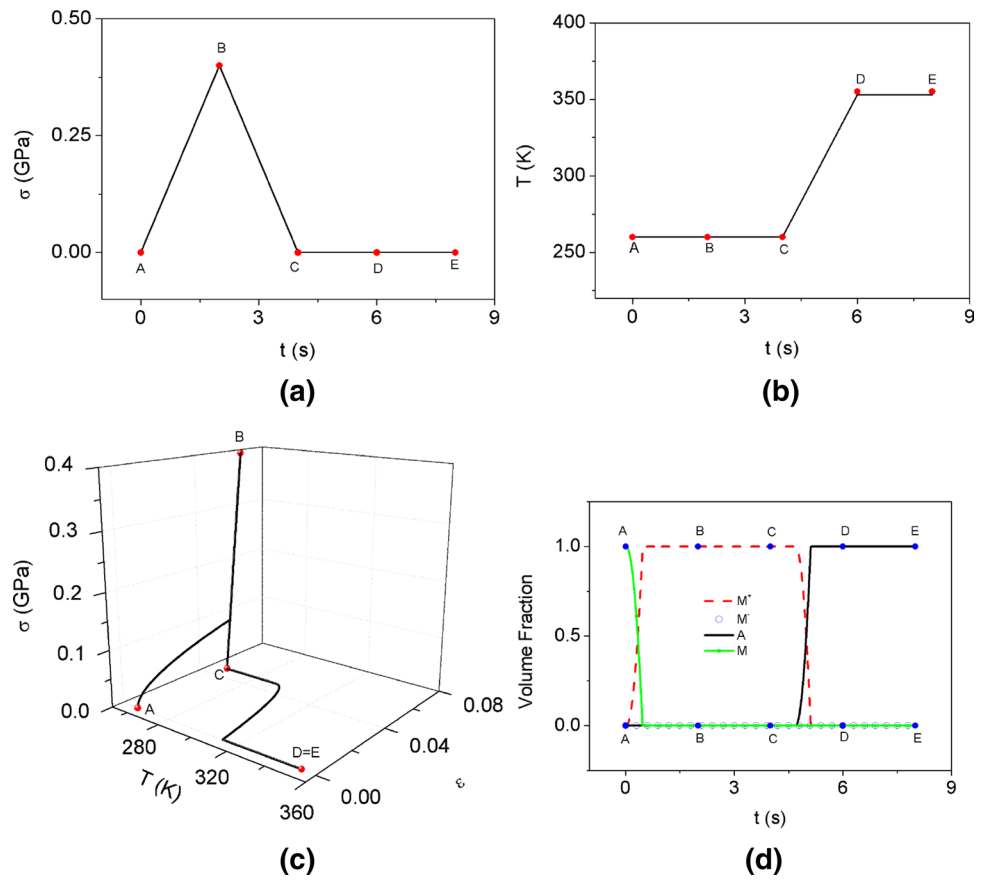
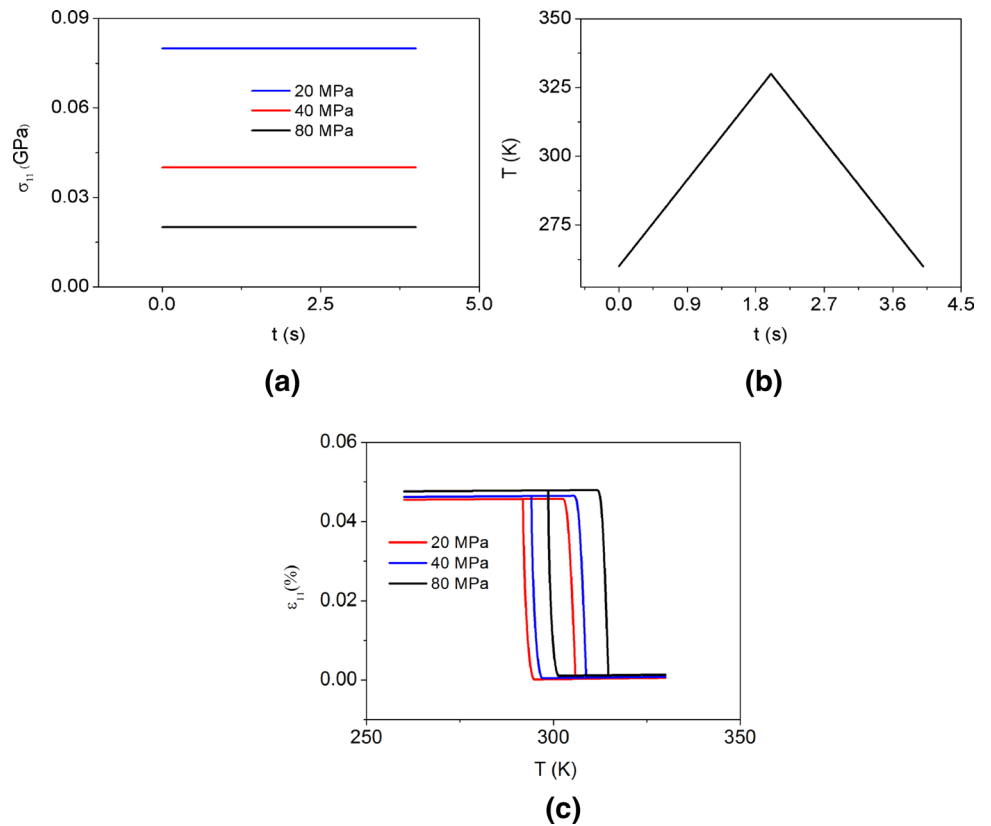


**Fig. 7** Temperature-induced phase transformation for different, constant stress loading. **a** Stress loading; **b** thermal loading; **c** strain–temperature curve



to a loading process that first, forms the major loop following the path ABC. This process causes austenite–martensite phase transformation, path AB, followed by the reverse transformation, path BC. Afterward, loading path CD promotes incomplete phase transformation, around 50 %. After that, the unloading path DE promotes an elastic response followed by a reverse transformation. Hence, a new increase on stress values, path EF, promotes an elastic response followed by a phase transformation. The same behavior occurs during unloading path FG. During loading path GH, phase transformation is completed and the major loop is reached. Finally, the unloading path HI promotes the complete reverse transformation and the SMA sample returns to the austenitic phase. It is important to observe that the model captures the tendency that a diagonal of the major loop defines critical phase transformation stress values of the minor loops [33].

### 4.2 Shape memory effect

Shape memory effect is now focused on. The SMA sample starts at  $T = 260$  K, temperature in which the martensitic phase is stable in a stress-free state. Figure 6a, b presents the thermomechanical loading–unloading process. Figure 6c presents the stress–strain–temperature curve showing the whole process while Fig. 6d presents the volume fractions evolution. Initially, the sample is subjected to a stress loading that causes martensitic reorientation represented by the transformation from the twinned martensite ( $M$ ) to detwinned martensite ( $M^+$ ), path AB. When the phase transformation finishes, a linear response is observed. Afterward, the sample is subjected to a stress unloading process, path BC. During this path, phase transformation does not take place and, as a consequence, the sample presents a residual strain, point C. Note that temperature is constant during this stress loading–unloading

**Fig. 8** Pseudoelastic and plastic behaviors considering a cyclic stress loading with constant maximum stress of 1.3 GPa imposed to the sample. **a** Loading history; **b** stress–strain curve; **c** volume fraction evolution; **d** plastic strains

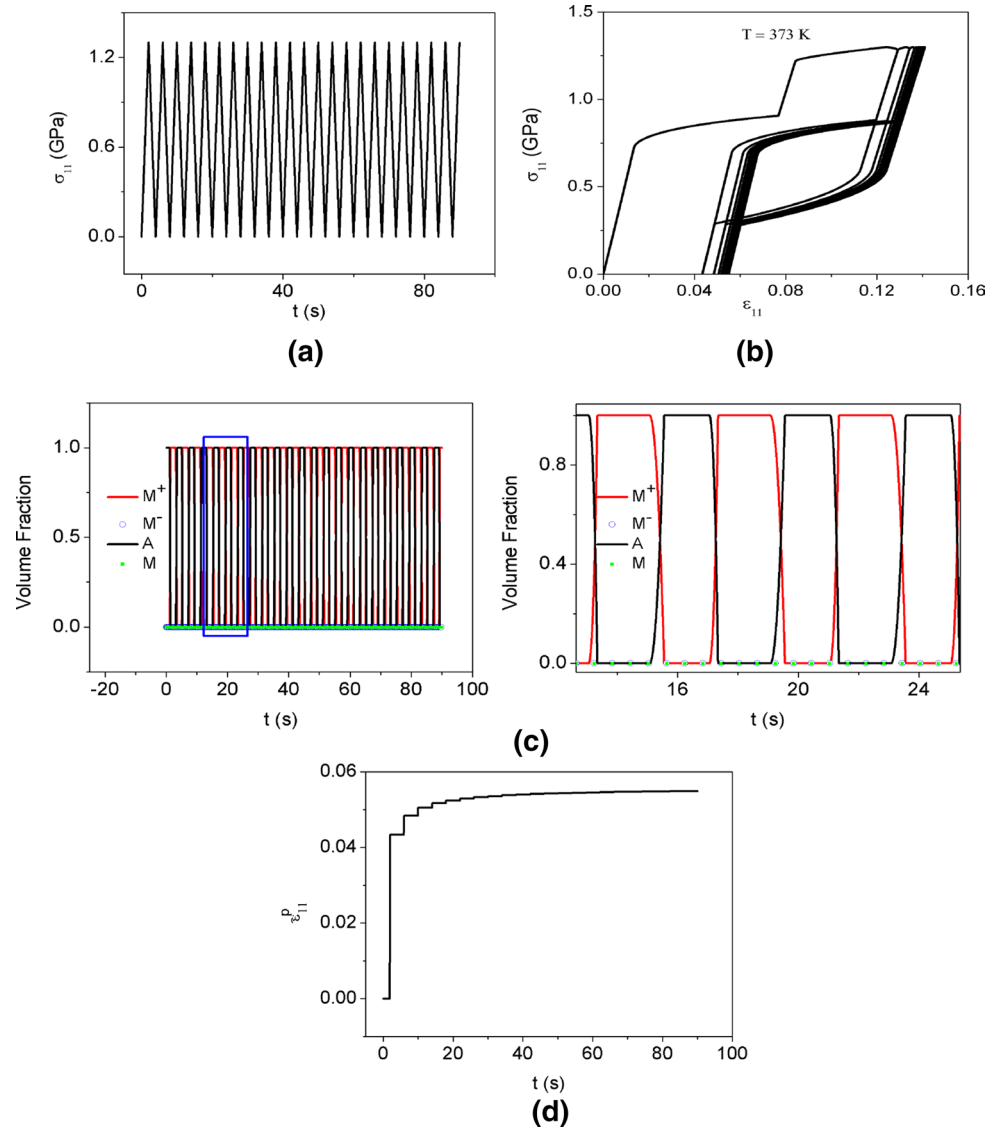
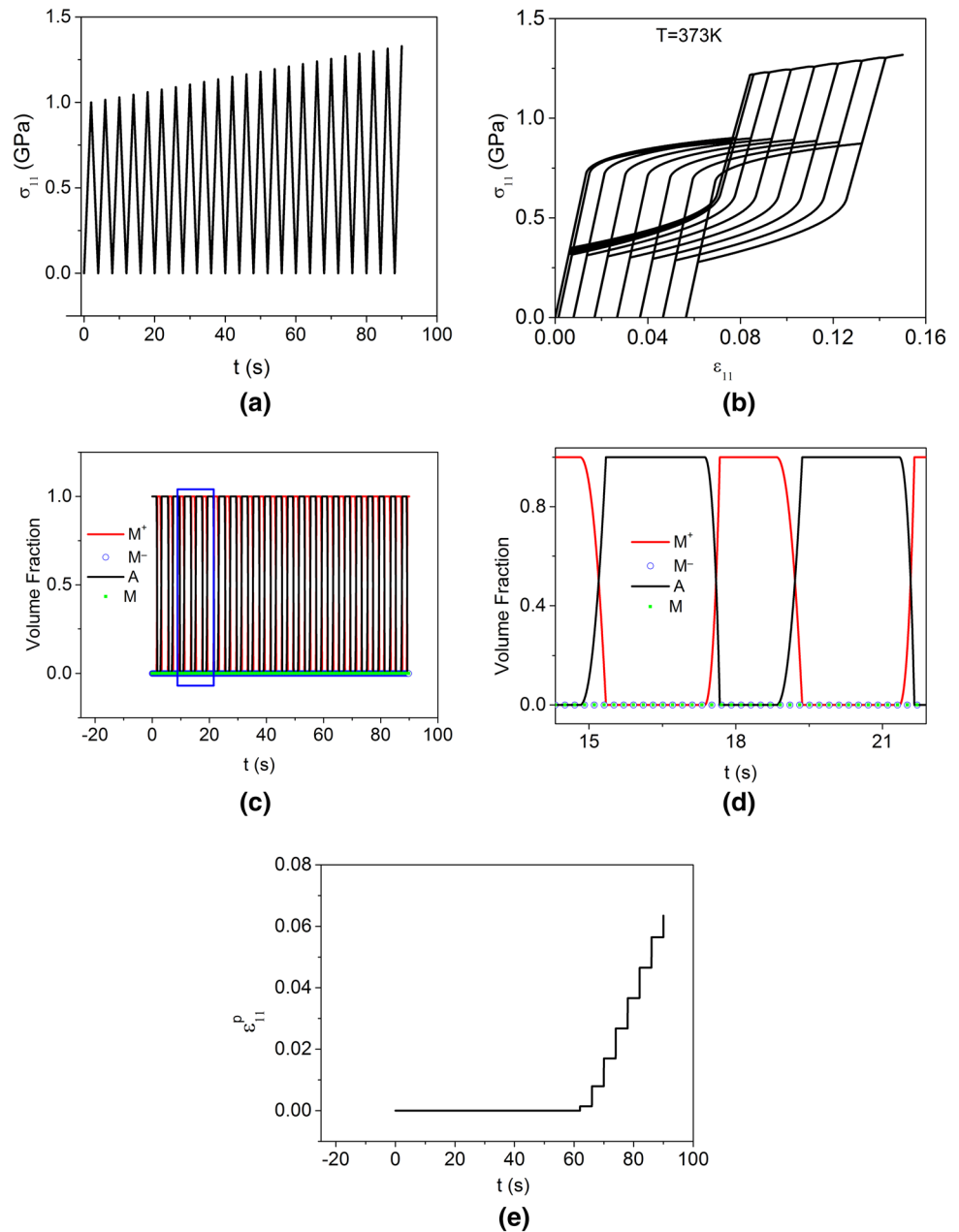


**Fig. 9** Pseudoelastic and plastic behaviors considering a stress loading history with maximum stress values that vary progressively from 1.0 to 1.3 GPa. **a** Loading history; **b** stress–strain curve; **c** volume fractions; **d** plastic strains



process, path ABC. The sample is then subjected to a thermal loading where temperature increase promotes phase transformation from martensite to austenite, path CDE. Once again, it should be noticed that the proposed model captures the general thermomechanical behavior for SMAs.

### 4.3 Temperature-induced phase transformation

The temperature-induced phase transformation is now focused on. Basically, tests are performed varying temperature, under a constant stress loading. Figure 7 shows

SMA response for this test. Figure 7a shows the stress loading process while Fig. 7b presents the thermal loading. Figure 7c presents the strain–temperature curve. Initially, the sample is at low temperature, below  $T_M$ . It is subjected to a constant stress load that induces the detwinned martensite formation. Afterward, the thermal loading promotes phase transformation from detwinned martensite to austenite. During unloading, the reverse transformation is induced. Note that the model is able to capture the typical experimental behavior where the SMA sample presents different hysteretic behaviors for each stress level.



**Fig. 10** Comparison between pure shear and equivalent tension–compression tests. **a** Stress–strain curve; **b** volume fraction evolution

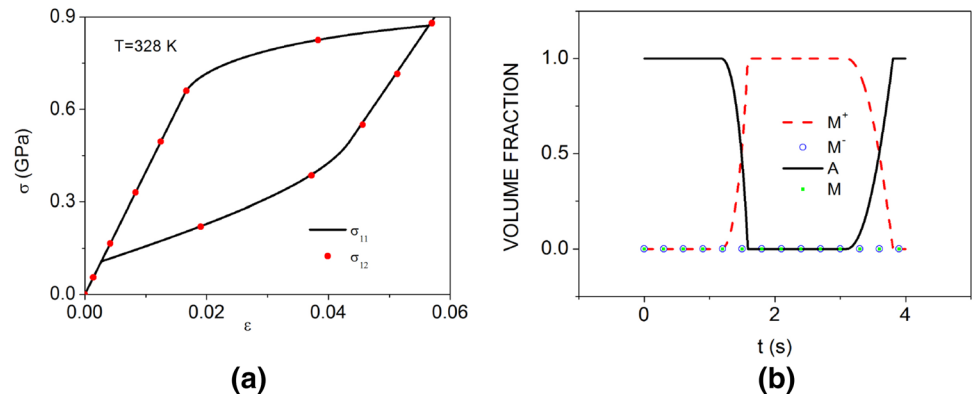


**Table 2** Model parameters based on numerical tests

$E^A$ (GPa)	$E^M$ (GPa)	$\Omega^A$ (MPa/K)	$\Omega^M$ (MPa/K)	$\alpha_N^h$ (MPa)	$\alpha_S^h$ (MPa)
65	29	0.74	0.17	0.016	0.015
$\alpha$ (MPa)	$\bar{L}_N$ (MPa)	$L_N$ (MPa)	$\bar{L}_N^A$ (MPa)	$L_N^A$ (MPa)	$\bar{L}_S$ (MPa)
1	0.01	7.05	2	21	0.005
$L_S$ (MPa)	$\bar{L}_S^A$ (MPa)	$L_S^A$ (MPa)	$T^M$ (K)	$T^F$ (K)	$\sigma_Y^M$ (GPa)
3.525	1	13	223	423	1
$\sigma_Y^{Ai}$ (GPa)	$\sigma_Y^{Af}$ (GPa)	$K^A$ (GPa)	$K^M$ (GPa)	$H^A$ (GPa)	$H^M$ (GPa)
0.8	0.3	1.4	0.4	4	1.1
$\eta^I$	$\eta^K$	$(\eta_L)_N$ (MPa s)	$(\eta_U)_N$ (MPa s)	$(\eta_L^A)_N$ (MPa s)	$(\eta_U^A)_N$ (MPa s)
−0.01	−0.01	2.4	2.4	2.4	0.8
$(\eta_L)_S$ (MPa s)	$(\eta_U)_S$ (MPa s)	$(\eta_U^A)_S$ (MPa s)	$(\eta_U^A)_S$ (MPa s)	$\nu^A$	$\nu^M$
1.9	1.9	1.9	0.65	0.36	0.36

### 4.4 Plasticity

The plastic behavior of an SMA sample is now of concern by assuming different loading processes. Initially, a cyclic stress loading with constant maximum stress of 1.3GPa is imposed to the sample. Figure 8a shows the stress loading history while Fig. 8b presents the stress–strain curve. Figure 8c shows the volume fraction evolution and Fig. 8d presents the plastic strain evolution. Note that plastic strains tend to stabilize due to the interaction of the kinematic and isotropic hardening. This promotes a stabilization of the stress–strain diagram in a specific hysteresis loop where volume fractions change from  $\beta^+$  to  $\beta^A$  and vice versa.

A different behavior is observed in Fig. 9 where loading history has maximum stress values that vary progressively from 1.0GPa to 1.3GPa. This change alters the interaction of the kinematic and isotropic hardening presenting a different behavior. Figure 9a shows the stress loading history while Fig. 9b presents stress–strain curve. Figure 9c shows the volume fraction evolution and Fig. 9d presents the

plastic strain evolution. Under this new condition, a different evolution occurs and the plastic strains do not stabilize during the process.

## 5 Numerical simulations: multiaxial tests

This section deals with numerical simulations of multiaxial tests. Initially, pure shear test is of concern, comparing shear stress loading with the equivalent tension–compression loading. Afterward, a coupled tension–torsion test is performed.

### 5.1 Pure shear test

The analysis of a pure shear stress test allows one to verify the coordinate invariance by establishing a comparison between this test and the equivalent tension–compression test ( $T$ – $C$ ). Therefore, two different situations are compared, expressed by the maximum values of the stress tensors employed in the loading history:

**Fig. 11** Uncoupled tests: **a** tension; **b** torsion

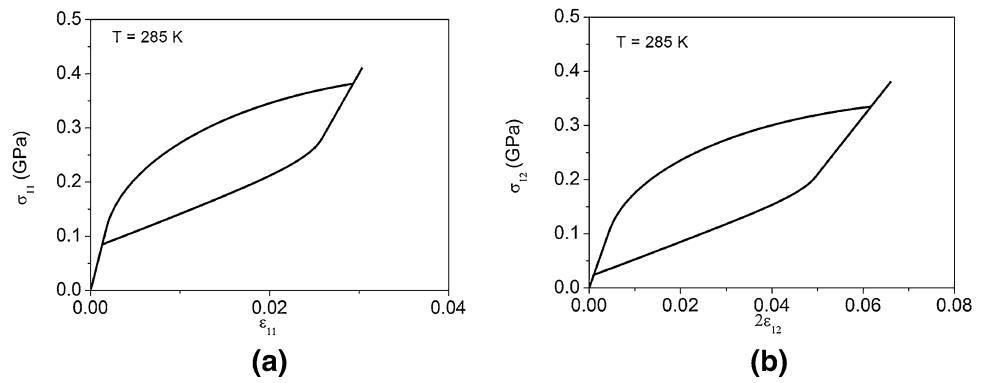


**Fig. 12** Loading process of the coupled tension–torsion test

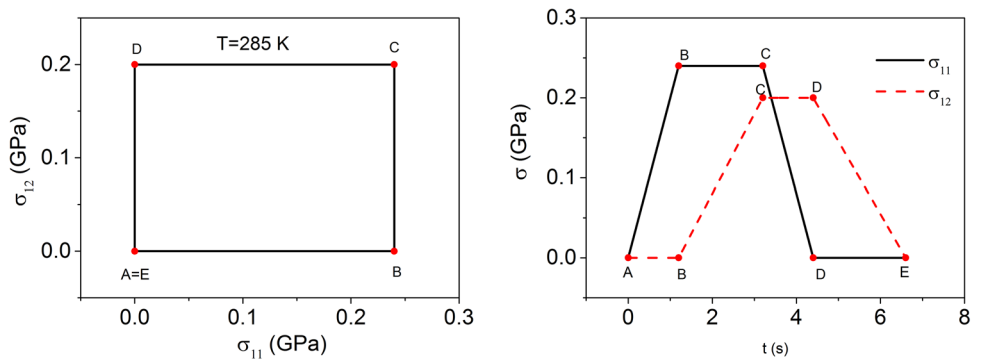
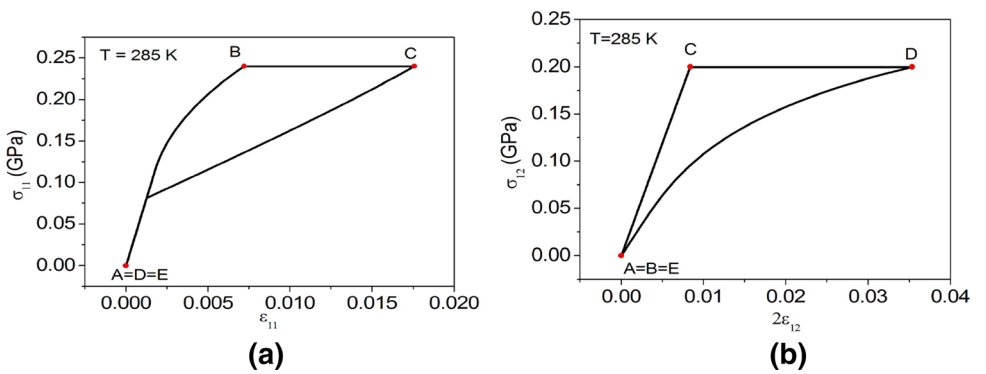


**Fig. 13** Tension–torsion coupled test: stress–strain curves. **a**  $\sigma_{11} \times \epsilon_{11}$ ; **b**  $\sigma_{12} \times 2\epsilon_{12}$



$$\sigma_{ij}^{Shear} = \begin{bmatrix} 0 & 1.1 & 0 \\ 1.1 & 0 & 0 \\ 0 & 0 & 0 \end{bmatrix} \text{ GPa}$$

$$\sigma_{ij}^{T-C} = \begin{bmatrix} 1.1 & 0 & 0 \\ 0 & -1.1 & 0 \\ 0 & 0 & 0 \end{bmatrix} \text{ GPa}$$

Both tests are carried out at temperature  $T = 328 \text{ K}$ . Figure 10 shows the SMA response presenting the stress–strain curves and the volume fractions evolution, comparing stress–strain curves obtained from both tests:  $\sigma_{11} \times \epsilon_{11}$  and  $\sigma_{12} \times \epsilon_{12}$ . The response is a typical pseudoelastic behavior and it is important to note that curves related to both tests are identical, confirming invariance of the coordinate system.

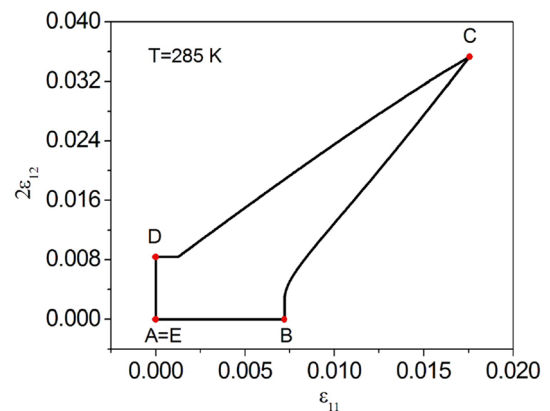


**Fig. 14** Tension–torsion coupled test: strain curve

### 5.2 Coupled tension–torsion test

A coupled tension–torsion test based on numerical data is now in focus. Initially, model parameters are adjusted by considering uniaxial tension and torsion tests, separately. Classical thermo-elasto-plastic parameters are employed as reference to adjust model parameters. Afterward, the coupled test is carried out using the adjusted parameters defined from the uncoupled tests. Table 2 presents model parameters employed to match uncoupled experimental tests. Besides,  $T_0 = 285$  K.

Results of the uncoupled tests are presented in Fig. 11 for both tension and torsion tests. Stress driving simulation is performed assuming a loading rate of 200 MPa/s.

Afterward, a tension–torsion coupled test is simulated using the same set of parameters. This test considers that an SMA austenitic sample is subjected to a loading process presented in Fig. 12 at a constant temperature ( $T = 285$  K). The path ABCDE represents a coupled tension–torsion loading. Initially, path AB represents a normal stress loading; path BC is a shear stress loading, without removing the normal stress; path CD represents the normal stress unloading; and finally, path DE represents the shear stress unloading. SMA

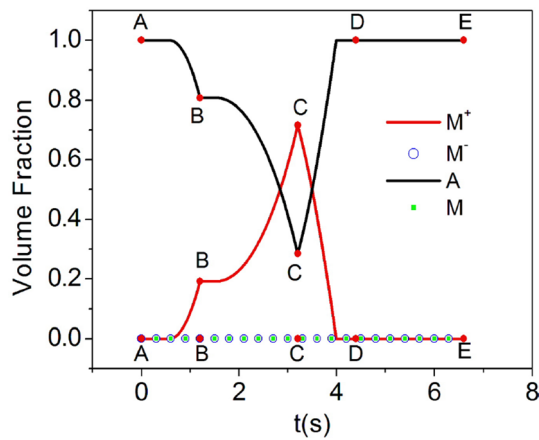


Fig. 15 Tension–torsion coupled test: volume fraction evolution

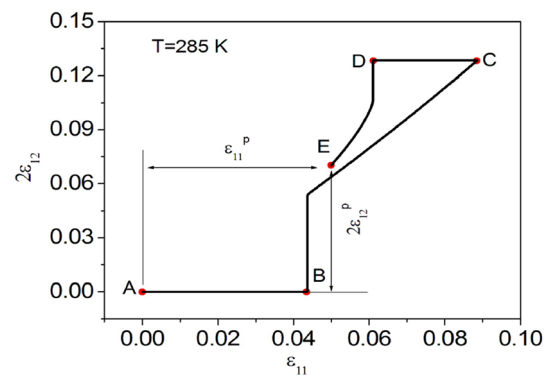


Fig. 18 Tension–torsion coupled test with plasticity: strain curve

Fig. 16 Loading process of the coupled tension–torsion test with plasticity

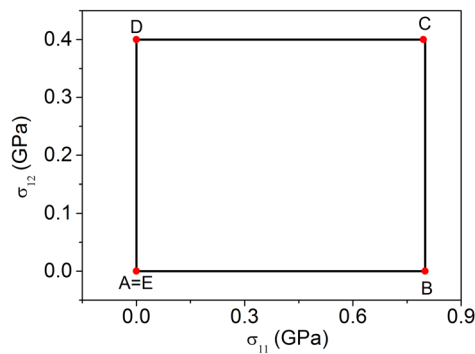
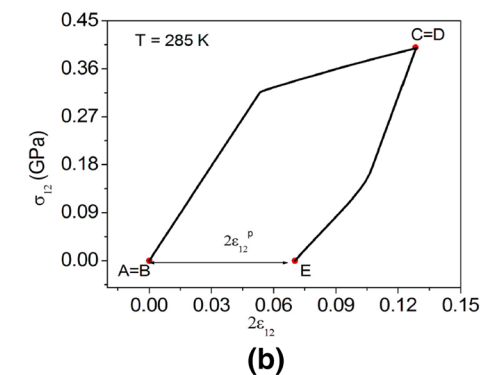
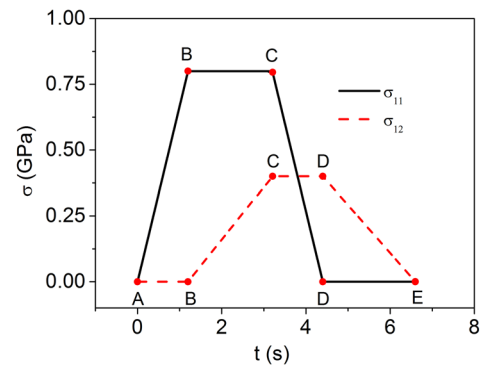
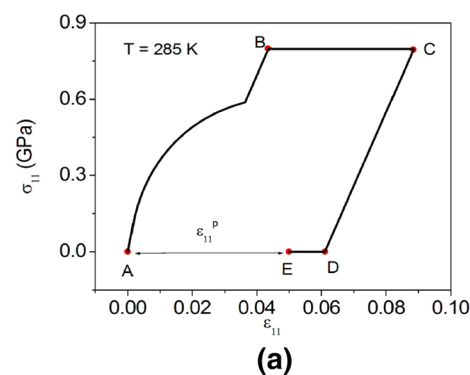
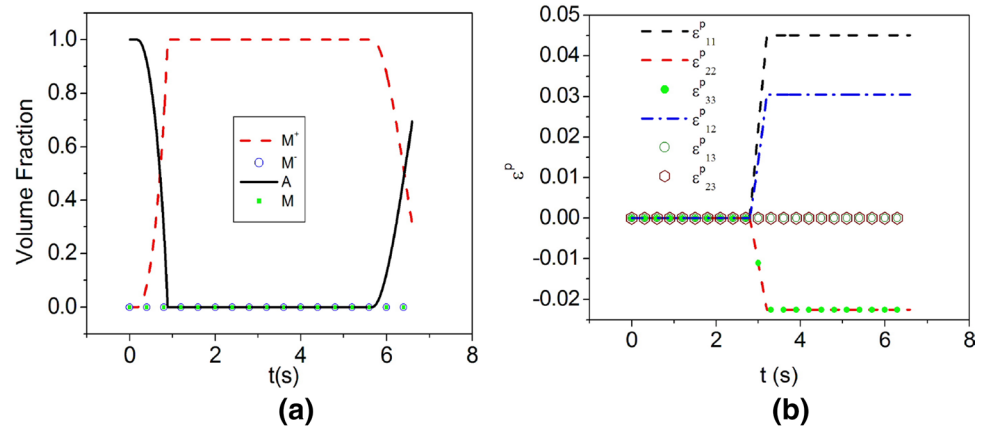


Fig. 17 Tension–torsion coupled test with plasticity: stress–strain curves. a  $\sigma_{11} \times \varepsilon_{11}$ ; b  $\sigma_{12} \times 2\varepsilon_{12}$



**Fig. 19** Tension–torsion coupled test with plasticity: **a** volume fraction evolution; **b** plastic strains evolution



response is presented in different ways. Stress–strain curves ( $\sigma_{11} \times \varepsilon_{11}$  and  $\sigma_{12} \times 2\varepsilon_{12}$ ) are presented in Fig. 13 while Fig. 14 presents the strain curve  $\varepsilon_{11} \times 2\varepsilon_{12}$ . Figure 15 presents volume fraction evolution that indicates phase transformations during the whole process. Initially, SMA sample is in austenitic phase (A). The normal stress loading promotes an incomplete phase transformation to detwinned martensite ( $M^+$ ). Afterward, loading path BC promotes more phase transformation. During the unloading path CD, the SMA sample starts a reverse transformation that finishes during the unloading path DE. It is possible to observe that the model captures the general qualitative behavior of the SMA in three-dimensional media with coupled loadings.

Plastic behavior of the tension–torsion coupled test is now of concern by assuming a situation similar to the previous test but increasing the stress values in order to reach the yield surface, showed in Fig. 16. Figures 17, 18 and 19 show the SMA three-dimensional behavior considering both phase transformation and plasticity. Figure 17 shows the stress–strain curves. Figure 18 shows the strain curve. Figure 19 presents the volume fraction and plastic strains evolution. Note that normal stress loading, path AB, promotes a complete phase transformation from austenite to detwinned martensite. After that, the shear stress loading, path BC, induces plastic strains, either normal or shear components. During normal stress unloading, reverse phase transformation does not take place. Nevertheless, this situation induces a decrease of normal plastic strain. The shear stress unloading causes the reverse phase transformation and the stabilization of plastic strains. Note that plastic effect changes the SMA behavior and the sample presents residual irreversible strains after the loading–unloading process.

## 6 Conclusions

This article presents a three-dimensional constitutive model for SMAs. Four macroscopic phases are

considered assuming different properties for austenitic and martensitic phases. Plastic phenomenon is considered by assuming both kinematic and isotropic hardening effects. An iterative numerical procedure based on the operator split technique is employed. Projection algorithm is employed for the phase transformation simulation while return mapping algorithm is employed for the plastic simulation. Numerical simulations are treated considering uniaxial and multiaxial tests. The uniaxial tests show the model capability to describe classical phenomena as pseudoelasticity, shape memory effect, internal subloops due to incomplete phase transformation and temperature-induced phase transformations. Moreover, some plastic phenomena are treated considering different loading histories that are responsible for distinct stabilization responses related to the interaction of the kinematic and isotropic hardenings. Concerning multiaxial tests, the coordinate invariance is confirmed by establishing a comparison between the pure shear test with the equivalent tension–compression test. Afterward, a coupled tension–torsion test is of concern. Model parameters are adjusted by considering tension and torsion tests separately and then the model is employed to simulate a tension–torsion coupled test. Plastic phenomenon is also investigated in this tension–torsion test showing that SMA sample presents residual irreversible strains after the loading–unloading process. In general, the model is able to capture the general thermomechanical behavior of uniaxial and multiaxial tests. Besides, the model flexibility should be highlighted since it describes all phenomena using the same set of parameters.

**Acknowledgments** The authors would like to acknowledge the support of the Brazilian Research Agencies CNPq, CAPES and FAPERJ and through the INCT-EIE (National Institute of Science and Technology—Smart Structures in Engineering) the CNPq and FAPEMIG. The Air Force Office of Scientific Research (AFOSR) is also acknowledged.

## References

1. Aguiar RAA, Savi MA, Pacheco PMCL (2010) Experimental and numerical investigations of shape memory alloy helical springs. *Smart Mater Struct* 19(2):025008
2. Andani MT, Elahinia M (2014) A rate dependent tension–torsion constitutive model for superelastic nitinol under non-proportional loading; a departure from von Mises equivalency. *Smart Mater Struct* 23:015012
3. Andani MT, Alipour A, Elahinia M (2013) Coupled rate-dependent superelastic behavior of shape memory alloy bars induced by combined axial-torsional loading: a semi-analytic modeling. *J Intell Mater Syst Struct* 24(16):1995–2007
4. Arghavani J, Auricchio F, Naghdabadi R, Reali A, Sohrabpour S (2010) A 3-D phenomenological constitutive model for shape memory alloys under multiaxial loadings. *Int J Plast* 26(7):976–991
5. Auricchio F, Reali A, Stefanelli U (2007) A three-dimensional model describing stress-induced solid phase transformation with permanent inelasticity. *Int J Plast* 23:207–226
6. Baêta-Neves AP, Savi MA, Pacheco PMCL (2004) On the Fremond’s constitutive model for shape memory alloys. *Mech Res Commun* 31:677–688
7. Bandeira EL, Savi MA, Monteiro PCC Jr, Netto TA (2006) Finite element analysis of shape memory alloy adaptive trusses with geometrical nonlinearities. *Arch Appl Mech* 76(3–4):133–144
8. Bessa WM, De Paula AS, Savi MA (2013) Adaptive fuzzy sliding mode control of smart structures. *Eur Phys J Spec Top* 222(7):1541–1551
9. Boyd J, Lagoudas DC (1996) A thermodynamical constitutive model for shape memory materials, part I: the monolithic shape memory alloy. *Int J Plast* 12(6):805–842
10. Brocca M, Brinson LC, Bazant ZP (2002) Three-dimensional constitutive model for shape memory alloys based on microplane model. *J Mech Phys Solids* 50:1051–1077
11. Chapman C, Eshghinejad A, Elahinia M (2011) Torsional behavior of NiTi wires and tubes: modeling and experimentation. *J Intell Mater Syst Struct* 22:1239–1248
12. Coleman BD, Noll W (1963) The thermodynamics of elastic materials with heat conduction and viscosity. *Arch Ration Mech Anal* 13(1):167–178
13. Coleman BD, Gurtin ME (1967) Thermodynamics with internal state variables. *J Chem Phys* 47(2):597–613
14. De Paula AS, dos Santos MVS, Savi MA, Bessa WM (2014) Controlling a shape memory alloy two-bar truss using delayed feedback method. *Int J Struct Stabil Dyn* 14(8):1440032
15. De Paula AS, Savi MA, Lagoudas DC (2012) Nonlinear dynamics of a SMA large-scale space structure. *J Braz Soc Mech Sci Eng XXXIV*:401–412
16. Eringen AC (1980) *Mechanics of continua*. Robert E. Krieger, New York
17. Fremond M (1996) *Shape memory alloy: a thermomechanical macroscopic theory*. CISM Courses and Lectures, New York, vol 351, pp 3–68
18. Fischer FD, Reisner G, Werner E, Tanaka K, Cailletaud G, Antretter T (2000) A new view on transformation induced plasticity. *Int J Plast* 16:723–748
19. Grabe C, Bruhns OT (2008) Tension–torsion tests of pseudoelastic, polycrystalline NiTi shape memory alloys under temperature control. *Mater Sci Eng A* 481:109–113
20. Hartl DJ, Chatzigeorgiou G, Lagoudas DC (2010) Three-dimensional modeling and numerical analysis of rate-dependent irrecoverable deformation in shape memory alloys. *Int J Plast* 26(10):1485–1507
21. Kalamkarov AL, Kolpakov AG (1997) *Analysis, design and optimization of composite structures*. Wiley, New York
22. Khalil W, Saint-Sulpice L, ArbabChirani S, Bouby C, Mikolajczak A, Ben Zineb T (2013) Experimental analysis of Fe-based shape memory alloy behavior under thermomechanical cyclic loading. *Mech Mater* 63:1–11
23. Lagoudas DC (2008) *Shape memory alloys: modeling and engineering applications*. Springer, New York
24. Lagoudas DC, Hartl D, Chemisky Y, Machado LG, Popov P (2011) Constitutive model for the numerical analysis of phase transformation in polycrystalline shape memory alloys. *Int J Plast* 32:155–183
25. Leblond JB, Devaux J, Devaux JC (1989) Mathematical Modeling of Transformation Plasticity in Steels I: Case of Ideal-Plastic Phases. *Int J Plast* 5(6):551–572
26. Lemaitre J, Charboche JL (1990) *Mechanics of solid materials*. Cambridge University Press, Cambridge
27. Machado LG, Savi MA (2003) Medical applications of shape memory alloys. *Braz J Med Biol Res* 36(6):302–306
28. Manach P, Favier D (1997) Shear and tensile thermomechanical behavior of near equiatomic NiTi alloy. *Mater Sci Eng A222*:45–57
29. McNaney JM, Imbeni V, Jung Y, Papadopoulos P, Ritchie RO (2007) An experimental study of the superelastic effect in a shape-memory nitinol alloy under biaxial loading. *Mech Mater* 35:969–986
30. Mehrabi R, Kadkhodaei M (2013) 3D phenomenological constitutive modeling of shape memory alloys based on microplane theory. *Smart Mater Struct* 22(2):025017
31. Mehrabi R, Kadkhodaei M, Andani MT, Elahinia M (2015) Microplane modeling of shape memory alloy tubes under tension, torsion, and proportional tension–torsion loading. *J Intell Mater Syst Struct* 26(2):144–155
32. Monteiro PCC Jr, Savi MA, Netto TA, Pacheco PMCL (2009) A phenomenological description of the thermomechanical coupling and the rate-dependent behavior of shape memory alloys. *J Intell Mater Syst Struct* 20(14):1675–1687
33. Muller I, Xu H (1991) On the pseudo-elastic hysteresis. *Acta Metall Mater* 39(3):263–271
34. Oliveira SA, Savi MA, Kalamkarov AL (2010) A three-dimensional constitutive model for shape memory alloys. *Arch Appl Mech* 80(10):1163–1175
35. Oliveira SA, Savi MA, Santos IF (2014) Uncertainty analysis of a one-dimensional constitutive model for shape memory alloy thermomechanical description. *Int J Appl Mech* 6(6):1450067
36. Ortiz M, Pinsky PM, Taylor RL (1983) Operator split methods for the numerical solution of the elastoplastic dynamic problem. *Comput Methods Appl Mech Eng* 39:137–157
37. Paiva A, Savi MA (2006) An overview of constitutive models for shape memory alloys. *Math Probl Eng* 2006:1–30. Article ID 56876
38. Paiva A, Savi MA, Braga AMB, Pacheco PMCL (2005) A constitutive model for shape memory alloys considering tensile-compressive asymmetry and plasticity. *Int J Solids Struct* 42(11–12):3439–3457
39. Panico M, Brinson LC (2007) A three-dimensional phenomenological model for martensite reorientation in shape memory alloy. *J Mech Phys Solids* 55(11):2491–2511
40. Popov P, Lagoudas DC (2007) A 3-D constitutive model for shape memory alloys incorporating pseudoelasticity and detwinning of self-accommodated martensite. *Int J Plast* 23:1679–1682
41. Rockafellar RT (1970) *Convex analysis*. Princeton Press, New Jersey
42. Saleeb AF, Dhakal B, Padula SA, Gaydos DJ (2013) Calibration of a three-dimensional multimechanism shape memory alloy material model for the prediction of the cyclic attraction character in binary NiTi alloys. *J Intell Mater Syst Struct* 24(1):70–88

43. Santos BC, Savi MA (2009) Nonlinear dynamics of a nonsmooth shape memory alloy oscillator. *Chaos Solitons Fractals* 40(1):197–209
44. Savi MA, Braga AMB (1993) Chaotic vibration of oscillator with shape memory. *J Braz Soc Mech Sci* 15(1):1–20
45. Savi MA, Paiva A, Baeta-Neves AP, Pacheco PMCL (2002) Phenomenological modeling and numerical simulation of shape memory: a thermo-plastic-phase transformation coupled model. *J Intell Mater Syst Struct* 3(5):261–273
46. Savi MA, Pacheco PMCL, Braga AMB (2002) Chaos in a shape memory two-bar truss. *Int J Non-Linear Mech* 37(8):1387–1395
47. Savi MA, Paiva A (2005) Describing internal subloops due to incomplete phase transformations in shape memory alloys. *Arch Appl Mech* 74(9):637–647
48. Savi MA, De Paula AS, Lagoudas DC (2011) Numerical investigation of an adaptive vibration absorber using shape memory alloys. *J Intell Mater Syst Struct* 22(1):67–80
49. Savi MA, Nogueira JB (2010) Nonlinear dynamics and chaos in a pseudoelastic two-bar truss. *Smart Mater Struct* 19(11):1–11, (Article 1150222010)
50. Savi MA (2015) Nonlinear dynamics and chaos of shape memory alloy systems. *Int J Non-Linear Mech* 70:2–19
51. Schroeder TA, Wayman CM (1977) The formation of martensite and the mechanism of the shape memory effect in single crystals of Cu–Zn alloys. *Acta Metall* 25:1375, (Article ID 1150222010)
52. Shaw JA, Kyriades S (1995) Thermomechanical aspects of Ni–Ti. *J Mech Phys Solids* 43(8):1243–1281
53. Silva LC, Savi MA, Paiva A (2013) Nonlinear dynamics of a rotordynamic nonsmooth shape memory alloy system. *J Sound Vib* 332(3–4):608–621
54. Simo JC, Hugles TJR (1998) *Computational inelasticity*. Springer, New York
55. Sitnikova E, Pavlovskaja E, Wiercigroch M, Savi MA (2010) Vibration reduction of the impact system by an SMA restraint: numerical studies. *Int J Non-Linear Mech* 45(9):837–849
56. Sittner P, Heller L, Pilch J, Sedlak P, Frost M, Chemisky Y, Duval A, Piotrowski B, Ben Zineb T, Patoor E, Auricchio F, Morganti S, Reali A, Rio G, Favier D, Liu Y, Gibeau E, LExcellent C, Boubakar L, Hartl D, Oehler S, Lagoudas DC, Van Humbeeck J (2009) Round robin SMA Modeling. In: ESOMAT 2009-8th European symposium on martensitic transformations. doi:10.1051/esomat/200908001
57. Sittner P, Hara Y, Tokuda M (1995) Experimental study on the thermoelastic martensitic transformation in shape memory alloy polycrystal induced by combined external forces. *Metall Mater Trans* 26A:2923–2935
58. Sittner P, Takakura M, Tokuda M (1997) Shape memory effects under combined forces. *Mater Sci Eng A* 234:216–219
59. Souza AC, Mamiya EN, Zouain N (1998) Three-dimensional model for solids undergoing stress-induced phase transformations. *Eur J Mech A Solids* 17:189–806
60. Tobushi H, Iwanaga N, Tanaka K, Hori T, Sawada T (1991) Deformation behavior of Ni–Ti shape memory alloy subjected to variable stress and temperature. *Contin Mech Thermodyn* 3:79–93
61. Tokuda M, Ye M, Takakura M, Sittner P (1999) Thermomechanical behavior of shape memory alloy under complex loading conditions. *Int J Plast* 15(2):223–239
62. Tokuda M, Ye M, Takakura M, Sittner P (1998) Calculation of mechanical behaviors of shape memory alloy under multi-axial loading conditions. *Int J Mech Sci* 40(2–3):227–235
63. Wang YF, Yue ZF, Wang J (2007) Experimental and numerical study of the superelastic behavior on NiTi thin-walled tube under biaxial loading. *Comput Mater Sci* 40(2):246–254
64. Zaki W, Moumni Z (2007) A three-dimensional model of the thermomechanical behavior of shape memory alloys. *J Mech Phys Solids*. doi:10.1016/j.jmps.2007.03.012
65. Zhang XD, Rogers CA, Liang C (1991) Modeling of two-way shape memory effect. *Smart Struct Mater ASME* 24:79–90
66. Zhou B (2012) A macroscopic constitutive model of shape memory alloy considering plasticity. *Mech Mater* 48:71–81